UCLouvain

École polytechnique de Louvain

Theoretical investigations on *N*-salicylideneaniline derivatives

Effects of mono- and di-N-substitutions on the phenylamino group

Author : **Razieh BAKHSHANDEHSERAJI**

Supervisors : **Benoît CHAMPAGNE, UNamur**

Readers : **Yoann OLIVIER, …, JOHAN WOUTERS**

Academic year 2019–2020

Advanced Master in Nanotechnologies

Summary

The reaction of condensation leading to the synthesis of N-salicylideneaniline derivatives is the target of this Master thesis and it has been investigated by using a broad range of quantum chemistry methods. N-salicylideneanilines are molecular switches, known for their photo- and thermochromisms. The objective of this work was to start from a well-studied compound, (E)-2-methoxy-6-(pyridine-3-yliminomethyl) phenol, and to consider isomers that differ by the number (1 or 2) and positions of the N atoms of the "pyridine" ring.

First, the energies of the condensation reaction to get the enol forms have been evaluated at the reference CCSD level of approximation, showing that the process is energetically favorable. Lower-level approximations have been assessed so that, within density functional theory, the double hybrid B2PLYP exchange-correlation functional appears as a reliable method. Then comes the ωB97X-D, which has the advantage to be computationally much cheaper. A detailed analysis of the "energies" of reaction (ΔE^0, ΔH^0, and ΔG^0) has shown that the electronic contributions are the driving forces to these quantities. Then, calculations performed at the MP2 level reveal that the most exothermic ($\Delta H^0 < 0$) and exergonic ($\Delta G^0 < 0$) condensations occur for the anils with a single N substitution. Then come the condensations with two nitrogen atoms, with at least one in position 3 (like in the reference compound). At the same level, it appears that for all N-salicylideneaniline derivatives except one the enol form is more stable (on the basis of ΔE^0 values) than the keto one and that further studies should be devoted to explain this observation.

Keywords: N-salicylideneanilines, thermodynamics of the reaction of condensation, quantum chemistry methods, assessment of exchange-correlation DFT functionals

Acknowledgements

I would like to thank the UCLouvain and UNamur for having given me the opportunity to do this Master Thesis. I would also like to thank the UNamur LCT (Laboratoire de Chimie Théorique) members, especially Pierre Beaujean for guidance and technical help they gave me all along this master thesis, as well as Professor Benoît Champagne for actively supervising the whole work. I would also like to thank Alireza Bagherpour and Tarcius Nascimento Ramos for their support during my master program. The calculations have been performed on the computers of the CECI and mostly those of the PTCI, for which I gratefully acknowledge the support of the F.R.S.-FNRS, of the Région Wallone, and of UNamur.

Table of content

I. GENERAL INTRODUCTION

N-salicylideneaniline derivatives (usually called anils) were first studied by Senier and Shepheard[1]. These molecules are prepared by the condensation of salicylaldehyde with primary amines. The attention to these types of compounds comes from the fact that they are able to undergo reversible proton transfer, leading to interesting properties such as thermo- and photo-chromism, making these molecules appropriate candidates for optical switches and storage devices[1]. This proton transfer defines an equilibrium, called tautomerism, between an enol-imine (OH) and a keto-enamine (NH) form, with the enol-imine form generally being the most stable form at room temperature[2]. As a result, the OH form of *N*-salicylideneanilines has been well-characterized, but until recently, few purely NH form had been structurally characterized[3]. For instance, the confirmation of a *N*-salicylideneaniline exclusively in the NH form in the solid-state has been controversial[4].

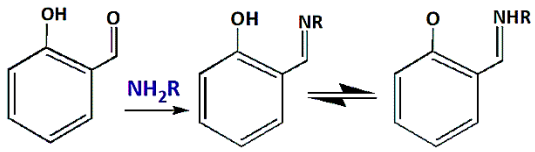

Scheme 1: Condensation of salicylaldehyde with a primary amine to form *N*-salicylideneanimine[1]

In the 1960s, Cohen and Schmidt investigated the relationship between structural and physical properties in detail. They suggested that crystals containing the molecules in a nonplanar conformation are photochromic while those with molecules in a planar conformation are not photochromic but can exhibit thermochromic properties[5]. In fact, *N*-salicylideneanilines are among the most common photo- and thermo-switchable molecules. They are also documented to exhibit both thermo- and photo-chromisms at the solid state[6]. These are illustrated in Fig. I.1 for a very simple anil derivative. Its thermochromism is associated to a thermal tautomeric equilibrium between the uncolored enol (which is a *cis* form) and the yellow *cis*-keto forms. On the other hand, photochromism arises from the photo-isomerization at 365 and 436 nm of both the enol and *cis*-keto forms to the red *trans*-keto form[7,8]. Other anil derivatives absorb at other wavelengths, as demonstrated by the large range of colors shown by these molecules[8,7].

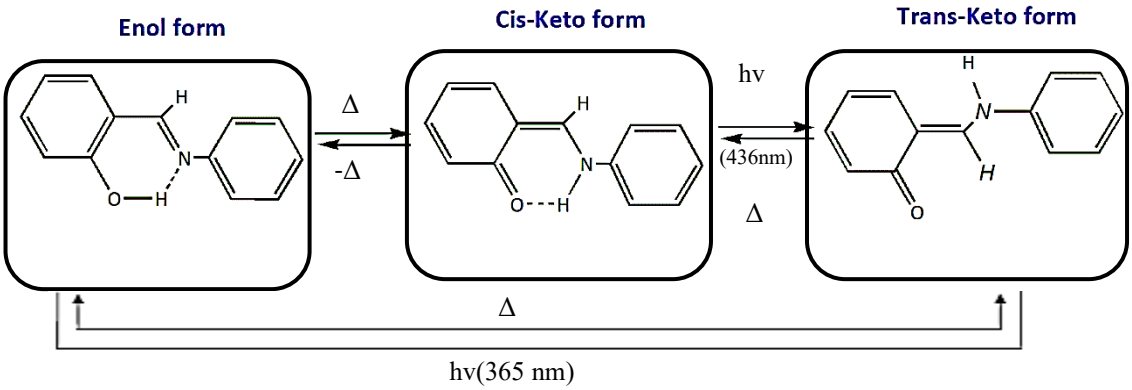

Fig.I.1**:** Thermochromic and photochromism of a typical N-salicylideneaniline[7].

Photochromic properties of *N*-salicylideneanilines, including color and thermal bleaching, are highly dependent on the molecular conformation and crystalline environment around the molecule. Until now, different methods such as chemical modification, mixing with polymers, zeolites, mesoporous

silica, cyclodextrins, cationic host matrix, clathrates, and bile acids, confining in a metal organic framework (MOF) and co-crystal formation through acid-base interactions have been reported to tune the structure and electronic properties of *N*-salicylidene-anilines, and therefore to change their photochromic reactivity[9].

In this Master thesis, we were particularly interested by *N*-salicylideneaniline derivatives that have been used in various fields such as nonlinear optics,[10] catalysis,[11] biology,[11] and several applications have been proposed (chemical sensors),[12] stimuli responsive polymers,[13] molecular machines,[14] information storage and displays[14]. This latter application is probably the most promising one thanks to the thermo- and photochromism switching ability of a few *N*-salicylideneaniline derivatives that occur in the solid-state and without fatigue[7].

N-Salicylideneaniline derivatives were firstly claimed to be thermochromic or photochromic but not both. This exclusive classification was recently clarified and *N*-salicylideneaniline derivatives were shown to be either photochromic and thermochromic or only thermochromic (except for few rare examples that are neither thermo- nor photo-chromic, and present a strong deep red coloration probably originating from a very large *cis*-keto form population)[7,15]. Being aware of the importance to predict these optical properties, a structure–property classification was proposed. Thermochromic compounds were observed as planar molecules that are closely packed in the crystal lattice, with a small dihedral angle between aromatic rings ($\Phi < 25°$)[7]. These planar structures are stabilized by strong π-π or C-H···π supramolecular interactions. Aromatic rings and imine groups are particularly involved in these interactions, assisted by the charge-transfer phenomenon. Thermo- and photochromic molecules were described as highly twisted molecules, with large dihedral angles ($\Phi \geq 25°$), packed within an open structure[7]. Interestingly, *N*-salicylideneaniline derivatives are only thermochromic in solution because of the low stability of the *trans*-keto form in this medium. Based on the above explanation *N*-salicylideneanilines have numerous applications, which are strongly influenced by their environment[16].

According to the high sensitivity of *N*-salicylideneaniline to the environmental conditions, many factors are able to change its properties, therefore, recognition of the optimized condition for *N*-salicylideneaniline derivatives plays a vital role in utilizing them in many fields such as optics, biology, etc. The sensitivity of these structures cannot prevent their usage. Besides the preparation or synthesis of these compounds and their physico-chemical characterizations, quantum chemistry methods have also been employed to provide complementary information, and to help in designing these multifunctional compounds. In that frame, determining the optimal quantum chemistry method for the investigation of *N*-salicylideneaniline derivatives is a preliminary step that should not be overcome. This encompasses the study of their structural and thermodynamical properties as well as different spectral signatures. To this purpose, in this master thesis, we focused on the thermodynamics of the condensation reactions as well as on structural aspects. In particular, we highlight the importance of the choice of theoretical model to describe these reactions.

II. METHODOLOGICAL AND COMPUTATIONAL ASPECTS

II.1. The Hartree-Fock method

The Hartree-Fock (HF) approach is a method for obtaining approximate total wave functions of many-electron systems. It has been applied successfully to many areas of quantum mechanics including atomic, molecular, and solid-state systems[17]. This method is an approximate mean-field method to solve the Schrodinger equation. It is the central starting point for most quantum chemistry methods that can describe many-electron systems more accurately, *i.e.* by including explicit electron-electron interactions, referred to as electron correlation[18]. The HF method is based on both the central field approximation and the variational principle.

The many-body Hamiltonian[19] of a molecule may be written in atomic units as

$$\hat{H} = -\frac{1}{2}\sum_{i}^{N_e}\nabla_i^2 - \sum_{i}^{N_e}\sum_{I}^{N_n}\frac{Z_I}{|\vec{r}_i - \vec{R}_I|} + \frac{1}{2}\sum_{i}^{N_e}\sum_{i\neq j}^{N_e}\frac{1}{|\vec{r}_i - \vec{r}_j|} + \frac{1}{2}\sum_{I}^{N_n}\sum_{I\neq J}^{N_n}\frac{Z_I Z_J}{|\vec{R}_I - \vec{R}_J|} \qquad (1)$$

As shown by Eq.1, the first term is the kinetic energy of the electrons, the second term corresponds to electrons-nucleus interaction, the third one shows electron-electron interaction and the forth term describes the nuclei repulsions. $|\vec{r}_i - \vec{R}_I|$is the distance between electron i and nucleus I, $|\vec{r}_i - \vec{r}_j|$ is the distance between electron i and electron j, and, similarly, $|\vec{R}_I - \vec{R}_J|$ is the distance between nuclei I and J. For the time being, we take the final term to be a constant and we only consider the electronic Hamiltonian, which is just

$$\hat{H}_e = -\frac{1}{2}\sum_{i}^{N_e}\nabla_i^2 - \sum_{i}^{N_e}\sum_{I}^{N_n}\frac{Z_I}{|\vec{r}_i - \vec{R}_I|} + \frac{1}{2}\sum_{i}^{N_e}\sum_{i\neq j}^{N_e}\frac{1}{|\vec{r}_i - \vec{r}_j|} \qquad (2)$$

In Eq. 2 the kinetic energy term and the nucleus-electron interaction term are sums of single-particle operators, each of which acts on a single electronic coordinate. The electron-electron interaction term on the other hand is a pair interaction and acts on pairs of electrons. To facilitate the upcoming developments, let's make the following definition[19]

$$\hat{H}_e = \sum_{i}\hat{h}_1(\vec{x_i}) + \frac{1}{2}\sum_{i\neq j}\hat{h}_2(\vec{x}_i, \vec{x}_j) \qquad (3)$$

where $\vec{x}_i$ is now a generalized coordinate that includes spatial as well as spin degrees of freedom.

The **Hartree-Fock** method is a variational wave function-based approach. Although it is a many-body technique, the approach followed is that of a single-particle picture, *i.e.* the electrons are considered as occupying single-particle orbitals making up the wave function. Each electron feels the presence of the other electrons indirectly through an effective potential. Each orbital, thus, is affected by the presence of the electrons in all the other occupied orbitals[19]. The starting point of the Hartree-Fock method is to write a wavefunction built from these single particle orbitals. The simplest wavefunction that can be formed from these orbitals is their simple product:

$$\phi(\vec{x}_1, .., \vec{x}_N) = \phi_1(\vec{x}_1)\phi_2(\vec{x}_2) \dots \phi_N(\vec{x}_N) \qquad (4)$$

This corresponds to the Hartree approximation and it is a straightforward task to calculate the variational lowest energy from Eq. 4. However, the Hartree wavefunction has a very important shortcoming, *i.e.* it fails to satisfy the antisymmetry condition, which states that a fermionic wavefunction changes sign under odd permutations of the electronic variables. In order to satisfy the antisymmetry condition, a more sophisticated form than that of the Hartree wavefunction is needed. The Slater determinant is the solution. So, the Hartree-Fock method consists in representing the N-electron wave function by a unique slater determinant $\psi(x_1,x_2,\ldots,x_N)$, built from one-electron wave functions, the spin-orbitals $\Theta_i(x)$

$$\psi(x_1, x_2, \ldots, x_N) = \psi^{HF}(x_1, x_2, \ldots, x_N) = \frac{1}{\sqrt{N!}} \begin{vmatrix} \Theta_1(x_1) & \Theta_2(x_1) & \cdots & \Theta_N(x_1) \\ & \vdots & \ddots & \vdots \\ \Theta_1(x_N) & \Theta_2(x_N) & \cdots & \Theta_N(x_N) \end{vmatrix} \quad (5)$$

where $\Theta_i(x) = \phi_i(r)\,\sigma_i(\omega)$ are products of spatial orbitals $\phi_i(r)$ and spin functions $\sigma_i(\omega)$. The spin function $\sigma_i(\omega)$ is either α or β, with ω the spin coordinate. The HF method assumes that a single determinant is a good approximation to the exact solution. These best spin-orbitals are determined by invoking the variational principle, *i.e.* they are optimized to minimize the system ground state electronic energy. This is achieved by solving the Hartree-Fock equation.

One of the shortcomings of the HF method is the neglect of explicit electron correlation. Electron correlation is mainly caused by the instantaneous interaction between electrons which is not treated in an explicit way in the HF method[20]. Therefore, several physical phenomena cannot be explained (or are poorly described) using the HF method, for example, the dissociation of molecules[20]

There are two types of electron correlation: **static (or non dynamic)** and **dynamic**. The static correlation is related to the behavior of the HF method at the dissociation limit of the molecule and deals with the long-range behavior of this approach. On the other hand, dynamic electron correlation is related to the electron repulsion term and its importance evolves as the inverse of the interelectronic distance. It is thus a short-range phenomenon[20]. However, it should be noted that *some* electron correlation in the HF method is included in an indirect manner by the consideration of the electronic motion in an effective potential field due to the nuclei and the rest of the electrons and due to the inclusion of electron spin[20]. Therefore, despite the known shortcomings, the HF method has been extensively used in quantum chemical calculations and has been quite successful for systems that are not extensive for electron correlation.

The correlation energy is defined as the energy difference between the exact nonrelativistic energy of a system and its HF energy. Electron correlation can be taken into account by the method of configuration interaction (CI) or by the many-body perturbation theory. The expansion of a molecular wavefunction in terms of Slater determinants is called configuration interaction (CI). The deficiency of an HF wavefunction in describing dissociation of a molecule can be largely corrected by a small (limited) CI calculation. Such correlation is called a non-dynamical (or static) correlation[20].

II.2 Linear combination of atomic orbitals and atomic basis sets

Before starting talking about CI method. It is necessary to discuss about an approximation known as the linear combination of atomic orbital (LCAO) method and the atomic basis sets. The LCAO

method is a quantum superposition of atomic orbitals (AOs) and a technique for describing efficiently the molecular orbitals (MOs)[21]. Indeed, to simplify the wavefunction description, we can expand the MOs into a set of predefined mathematical functions, which can represent the atomic orbitals, as shown in the following equation

$$\phi_i = \sum_n C_{ni}\varphi_n. \quad (6)$$

where the φ_n represents the n-th atomic orbital and ϕ_i the i-th molecular orbital. The C_{ni} are the expansion or LCAO coefficients, i.e. the weights of the contributions of the atomic orbitals to the molecular orbital. In a HF calculation, the MOs are calculated so that the best ground state wavefunction is determined. When using the LCAO approximation, since the AOs are known, solving the HF equation consists in searching for the best LCAO coefficients[22].

As a matter of fact, within the LCAO method, it is necessary to define or to choose a set of AOs, which is usually known as an atomic orbital basis set.

During the years, a huge collection of basis sets was generated in the context of wave function-based calculations. The detailed parameters of the atomic orbital basis sets involved in Gaussian can be found easily online, see [23] They are therefore not shown here, nor in appendix. Considering the importance of the number of basis functions in the computational cost and in the quality of the results, the objective of this section will be to describe in an introductory way the use of the basis functions sets.

In most calculations, the set is almost universally chosen to consist of so-called Cartesian Gaussian-type-orbitals **(GTO)**. Because very efficient algorithms exist for analytically calculating the huge number of four-center-two-electron integrals occurring in the Coulomb and HF-exchange terms, the GTO basis functions in HF and related methods is motivated by computational advantages[24]. On the other hand, natural choice of basis functions from a physical perspective is Slater-type-orbitals (STO). They are simple exponentials that mimic the exact eigenfunctions of the hydrogen atom. Should be mentioned that, unlike the GTO functions, Slater-type-orbitals represent the correct cusp behavior at $r \rightarrow 0$ with a discontinuous derivative (while a GTO has a slope of zero) and the desired exponential decay in the tail regions as $r \rightarrow \infty$ (GTO fall off more rapidly). This is why linear combinations (called contractions) of Gaussian functions are used to describe each AO. The simplest and least accurate expansions of the molecular orbitals utilize only one basis function (or rather one contraction of GTO) for each atomic orbital up to and including the valence orbitals. These basis sets are for obvious reasons called minimal sets. STO-nG, is the most common minimal basis set where **n** is an integer representing the number of Gaussian primitive functions comprising a single basis function. For a C atom, this basis set consists of five functions, one for describing the 1s and 2s atomic orbitals and three functions for the 2p shell (p_x, p_y, and p_z), so it is logical if they cannot show accurate results[23].

Bonds are mostly described by valence electrons. So, to go beyond minimal basis sets, it is common to represent valence orbitals by more than one basis function (each of which can in turn be composed of a fixed linear combination of primitive Gaussian functions). When there are multiple basis functions corresponding to each valence atomic orbital basis sets are called valence double, triple, quadruple-ζ and so on, basis sets (ζ is employed because it was commonly used to represent the exponent of an STO basis function)[22]. Since these basis functions have different spatial extents, their

combination allows the electron density to adjust its spatial extent as a function of a particular molecular environment[24]. On the other hand, minimal basis sets lack this flexibility to adjust to different molecular environments.

Ones of the most successful basis sets are those developed by Dunning and coworkers,[25] since they have been designed for obtaining converging post-Hartree–Fock results, i.e. systematically to converge towards the complete basis set limit using empirical extrapolation techniques. For first- and second-row atoms, these basis sets are cc-pVNZ where N = D, T, Q, 5, 6,... (D = double, T = triple, etc.). The 'cc-p' and the 'V' means 'correlation-consistent polarized' and valence basis sets. They include successively larger shells of polarization functions (d, f, g, etc.). More recently these 'correlation-consistent polarized' basis sets have become widely used and are the current state of the art for correlated or post-Hartree–Fock calculations [24]

In summary, our basis set choice should be "balanced": the basis set should be extended or flexible enough to describe the targeted properties of the molecules but not unnecessarily large because it would result in too large computational costs. So, we decided use the cc-pVTZ basis set for the geometry optimization as well as for the evaluation of the thermodynamical properties, at the different levels of approximation.

II.3. The configuration Interaction method

Configuration interaction (CI) theory has dominated the first 50 years of quantum chemistry before it was replaced by many-body perturbation theory and coupled cluster theory. However, even today it plays an important role in the education of everybody who wants to enter the realm of quantum chemistry[26]. In this method, the single determinant Hartree-Fock wave function is extended to a wave function composed of a linear combination of many determinants in which the coefficients are variationally optimized. These determinants are set up by determinant of the electronic ground state (ψ_0), that was previously obtained by running a Hartree-Fock calculation, by promoting one or more electron from occupied and virtual (unoccupied) levels. Therefore, singly–excited configuration (ψ_i^a) is obtained by substituting in the determinant the Θ_i spin-orbital that is occupied in the ground state by the Θ_a spin-orbital that is unoccupied in the ground state. This illustrates an excitation of an electron from Θ_i to Θ_a. Double–excited configurations are obtained by carrying out a double excitation and so on for higher-order substitutions. Eq. 7 shown the CI general wave function.

$$\psi = C_0\psi_0 + \sum_{i}^{occ}\sum_{a}^{unocc} C_i^a\psi_i^a + \sum_{i>j}^{occ}\sum_{a>b}^{unocc} C_{ij}^{ab}\psi_{ij}^{ab} + \sum_{i>j>k}^{occ}\sum_{a>b>c}^{unocc} C_{ijk}^{abc}\psi_{ijk}^{abc} + \cdots \qquad (7)$$

In this way, a CID (CI with all D excitations) wavefunction can be generated:

$$|\psi_{CID}> = C_0|\psi_0> + \sum_{i>j}^{a>b} C_{ij}^{ab}|\psi_{ij}^{ab}> \qquad (8)$$

where C_0 is the coefficient of the HF reference, which can be one or close to one depending on which normalization is used. The C^{ab}_{ij} are the mixing coefficients of the excited configurations. Hence, the CID wavefunction is expressed as a linear combination of the ground state HF Slater determinant and

all possible D-excited Slater determinants. The CID weighting coefficients C^{ab}_{ij} are determined by a variational approach during which the HF orbitals are kept frozen. The resulting CID energy is lower than the HF energy, however still an upper bound to the exact energy [26]. In the same way, the wave function of CISD, CISDT,.. will be specified.

Two characteristics of the CI method make it particularly attractive and important. First, unlike methods which rely on more restricted forms of trial wave functions (such as self-consistent field, separated pairs, etc.), it is capable, in principle, of providing accurate solutions of the nonrelativistic, clamped nuclei Schrödinger equation. Second, it is a general method, applicable in principle to any stationary state of an atomic or molecular system. While the qualification "in principle" in the above statements is significant, because of the slow convergence of the CI expansion and of difficulties in dealing with highly excited states, it should be seen in the context of the very rapid improvement in our capabilities for such calculations over the last decades[27].

Note that the CI method is based on two consecutive variational steps, one for optimizing the molecular orbitals (LCAO coefficients, HF method) of the reference (ground state) configuration and a second for optimizing the CI expansion coefficients but the CI method is not fully variational because these two sets of parameters are not optimized simultaneously. One of the drawbacks of the CI methods, when truncated, is the lack of size-consistency. Size-consistency error is characterized by correlation energy that does not scale properly with the size of the system, more rigorously, when the (correlation) energy of a system containing N non-interacting molecules is not equal to the sum of the energies of the N molecules considered individually.

The best molecular electronic wavefunction that can be calculated using a given basis set is obtained by a full CI calculation. However, the application of full CI for systems with more than a few atoms is not yet possible. On the other hand, limiting the number of configurations may result in a wavefunction that is not size consistent. For example, the configuration interaction-singles (CIS) method adds only single excitations, CID adds only double excitations, CISD adds both single and double excitations while CISDT includes up to triple excitations to the HF determinant.

II.4. Møller-Plesset perturbation theory

Perturbation theory has been used since the early days of quantum chemistry to obtain electron correlation-corrected descriptions of the electronic structure of atoms and molecules[28]. In 1934, Møller and Plesset described how the Hartree–Fock (HF) method can be corrected for electron pair correlation by using second-order perturbation theory[29]. The development of Møller–Plesset perturbation theory (MPPT) has seen four different periods in almost 80 years[28]. In the first 40 years (period 1), MPPT was largely ignored because the focus of quantum chemists was on variational methods theories with the upper bound property such as HF or configuration interaction (CI)[28]. After the development of many-body perturbation theory by theoretical physicists in the 1950s and 1960s, a second 20-year long period started, during which MPn methods up to order n=6 were developed and computer-programmed and MP2, MP3, MP4 and MP5 could be used by quantum chemists shortly after they had been worked out[28]. In the late 1980s and in the 1990s (period 3), shortcomings of MPPT became obvious, especially the sometimes erratic or even divergent behavior of the MPn

series. The physical usefulness of MPPT was questioned and it was suggested to abandon the theory. Since the 1990s (period 4), the focus of method development work has been almost exclusively on MP2[28].

Møller–Plesset perturbation theory (MPPT) constitutes the alternative to the variational CI approaches. It is one of several quantum chemistry post-Hartree–Fock methods in the field of computational chemistry. It employs the Rayleigh-Schrodinger perturbation theory to the problem of electron correlation. As presented in the material below, it allows determining the wavefunctions and energies of a perturbed system, provided the wavefunctions and energies are known for the unperturbed one. The unperturbed system in MPPT correspond to the Hartree-Fock solution and its zero-order (unperturbed) Hamiltonian corresponds to the sum of the one-electron Fock operators[30]:

$$\hat{H}_0 = \sum_{i=1}^{N_e} (h_i + v_i^{HF}) = \sum_{i=1}^{N_e} f_i \qquad (9)$$

The wave function in this method is provided by Slater determinants constructed from the HF MOs, occupied and/or unoccupied in the Hartree-Fock ground state determinant. Their corresponding energies are given by the sum of the energies of those orbitals constituting a given determinant. The perturbed Hamiltonian is the full Hamiltonian, containing the kinetic energy terms as well as the electron-electron repulsion terms. The perturbation, $\lambda\hat{w}$, is introduced as the difference between the perturbed and unperturbed Hamiltonians, reads:

$$\lambda\hat{w} = \hat{H} - \hat{H}_0 \ = \frac{1}{2}\sum_{i,j\ i\neq j}^{N_e} \frac{1}{|r_i - r_j|} - \sum_{i=1}^{N_e} v_i^{HF} \qquad (10)$$

v_i^{HF} is the Fock potential containing the Coulomb and exchange terms. According to this starting point the successive correction to energies and wavefunctions can be evaluated. The following expressions concentrate on the ground state and wave function but the method can be extended to other ones:

$$\psi_0 = \psi_0^{(0)} + \psi_0^{(1)} + \psi_0^{(2)} + \cdots \qquad (11)$$

$$E_0 = E_0^{(0)} + E_0^{(1)} + E_0^{(2)} + \cdots \qquad (12)$$

Therefore, by RSPT expression and using integration rules, one gets successive approximations to the energy and wavefunction. The ground state energy (0^{th} order) is simply the sum of the energies of the occupied MOs:

$$E_0^{(0)} = < \psi_0^{(0)} |\hat{H}_0| \psi_0^{(0)} > = \sum_i^N \varepsilon_i \qquad (13)$$

Based on the previous explanation the 1^{st} order correction brings Coulomb and exchange terms that are over-counted(doubly) so $E_0^{(1)}$ can be written

$$E_0^{(1)} = -\frac{1}{2}\sum_i^N \sum_j^N < ij||ij > \qquad (14)$$

The next step consists in writing the 1st order correction to the ground state wavefunction,

$$\psi_0^{(1)} = \sum_{k\neq 0}^{N} \frac{< \psi_k^{(0)} | \hat{w} | \psi_0^{(0)} >}{E_0^{(0)} - E_k^{(0)}} \psi_k^{(0)} \quad (15)$$

where the sum runs over all the excited configurations, singly-excited, doubly-excited,….Since the perturbation operator, $\hat{w}$, only contains one-and two-electron operators and, accounting for Brilloun's theorem, the sum over k can be reduced to a summation over the doubly-excited configurations only:

$$\psi_0^{(1)} = \sum_{i>j}\sum_{a>b} \frac{< \psi_{ij}^{ab(0)} | \hat{w} | \psi_0^{(0)} >}{E_0^{(0)} - E_{ij}^{ab(0)}} \psi_{ij}^{ab(0)} = \sum_{i>j}\sum_{a>b} \frac{< ab||ij >}{\varepsilon_i + \varepsilon_j - \varepsilon_a - \varepsilon_b} \psi_{ij}^{ab(0)} \quad (16)$$

This allows writing the 2nd order correction to the energy:

$$E_0^{(2)} = \sum_{j\neq 0} \frac{| < \psi_j^{(0)} | \hat{w} | \psi_0^{(0)} > |^2}{E_0^{(0)} - E_j^{(0)}} = \sum_{i>j}\sum_{a>b} \frac{| < ab||ij > |^2}{\varepsilon_i + \varepsilon_j - \varepsilon_a - \varepsilon_b} \quad (17)$$

This result is the most important because 2nd order correction is, within MPPT, the first correction to HF energy, and generally the dominant one. The process can be pushed further to express the 2nd order correction to the wavefunction and the 3rd order correction to energy. For both, again, only the doubles contribute but the situation gets different for the higher-order terms. Second (MP2), third (MP3), and fourth (MP4) order Møller–Plesset calculations are standard levels used in calculating small systems and are implemented in many computational chemistry codes. Higher-level MP calculations, generally only MP5, are possible in some codes. However, they are rarely used because of their cost[31–34].

Systematic studies of MP perturbation theory have shown that it is not necessarily a convergent theory at high orders. Convergence can be slow, rapid, oscillatory, regular, highly erratic, or simply non-existent, depending on the precise chemical system or basis set[35]. The density matrix for the first-order and higher MP2 wavefunction is of the type known as response density, which differs from the more usual expectation value density[36]. The eigenvalues of the response density matrix (which are the occupation numbers of the MP2 natural orbitals) can, therefore, be greater than 2 or negative. Unphysical numbers are a sign of a divergent perturbation expansion. Additionally, various important molecular properties calculated at MP3 and MP4 levels are no better than their MP2 counterparts, even for small molecules[30]. This is why, in the present work, MP2 will be used as our second reference method because it is computationally relatively cheap for evaluating the energy as well as the thermal corrections to the enthalpy, entropy, and Gibbs enthalpy while the higher-order MP schemes will also be employed for comparison purpose when assessing the role of successive higher-order electron correlation corrections.

II.5. The Coupled-Cluster Method

Coupled cluster (CC) theory provides a compelling framework of approximate infinite-order perturbation theory, in the form of an exponential of cluster operators describing the true quantum many-body effects of the electronic wave function at a computational cost that, despite being

significantly more expensive than mean-field methods, scales polynomially with the system size. The hierarchy of size-extensive approximate methods established in the framework of CC theory achieves systematic improvability for many materials properties[37]. Coupled cluster theory was proposed by Coester and Kümmel initially[37]. In the 1960s Cizek and Paldus introduced the method for electron correlation[38] and since then it has become a widely used electronic structure theory method for quantum chemical calculations on systems that do not exhibit strong static correlation[37]. The wavefunction amplitudes are obtained by solving a set of non-linear equations that can be derived using different methods including second quantization in combination with Wick's theorem, Slater rules or diagrammatic techniques[37]. Coupled cluster theory uses an exponential ansatz of cluster operators for the many-electron wavefunction:

$$|\psi^{CC}>= e^{\hat{T}}\psi^{HF} \qquad (18)$$

where ψ^{HF} is a single Slater determinant constructed from the Hartree-Fock one-electron orbitals that best approximates the ground state energy of a many-electron system[37]. This is known the exponential ansatz coupled-cluster theory. $\hat{T}$ is the (non-Hermitian) cluster operator, that contains all single, double, … excitation operators. Like in the CI theory, truncations have to be introduced. In CI, the wavefunction expansion was truncated beyond the doubles, triples, … leading to CISD and CISDT levels of approximation. In a similar way, in CC, the $\hat{T}$ expansion is truncated, after the single and the double excitations, which corresponds to the CCSD level of approximation. The CCSD method includes all single and double excitations in the cluster operator whereas the CISD method includes all single and doubly-excited determinants. Therefore, the first terms of CCSD is:

$$\left|CCSD>= |\psi_0> +\hat{T}_1|\psi_0> +\left(\hat{T}_2 +\frac{1}{2}\hat{T}_1^{\,2}\right)\right|\psi_0$$
$$> +\left(\hat{T}_2\hat{T}_1 +\frac{1}{6}\hat{T}_1^{\,3}\right)\left|\psi_0> +\left(\frac{1}{2}\hat{T}_2^{\,2} +\frac{1}{2}\hat{T}_2\hat{T}_1^{\,2} +\frac{1}{24}\hat{T}_1^{4}\right)\right|\psi_0> \qquad (19)$$

Many more electron correlation terms are included in the CCSD wavefunction than in the CISD one, moreover, the wavefunction product ensures size-consistency which is not the case for truncated CI. In the present work, CCSD is our reference method.

II.6. Density functional theory

Density functional theory (DFT) was developed to calculate the electronic states of solids containing huge numbers of electrons. In the earliest years, DFT was, therefore, used only for calculations of band structure and other properties of solids[39]. Since the 1990s DFT methods became central in many quantum chemistry calculations. Today by understanding the many aspects of it as well as further developments, it has become the predominant method. Computational chemistry is aimed mainly at describing chemical reactions and properties. Because chemical reactions are usually associated with electron transfers between many different molecular moieties, highly sophisticated methods are required, incorporating electron correlation (well-balanced dynamical and nondynamical correlations) for quantitative estimates. Therefore, Quantum chemists have focused on how to incorporate high-level electron correlations efficiently for several decades. [39]. So, to achieve this

purpose, various methods have been developed with the difference mainly in the approaches for sorting out electron configurations to incorporate electron correlations efficiently. Conventional methods that used before DFT required much computational time so that it was difficult to calculate the electronic states of large molecules[39]. For the reason that DFT can incorporate well-balanced static and dynamic electron correlation simply via the use of exchange-correlation functionals of the electron density, it enables to calculate chemical reaction energy diagrams quantitatively, with computational times equivalent or less than those for the Hartree–Fock method[39]. So due to its remarkable properties of the DFT method, this method became an important method in quantum chemistry. DFT method allows us to sidestep that computational difficulty by focusing on the electron density, instead of the many-body wave function. The underlying principle of DFT is that the total energy of any system is a unique functional of the electron density. Hence it is unnecessary to compute the full many-body wave function of the system. However, the precise functional dependence of the energy on the density is not known [40].

DFT is a remarkable theory that allows one to replace the complicated N-electron wave function $\psi(x_1, x_2, \ldots x_N)$ and the associated Schrödinger equation by the much simpler electron density, $\rho(r)$, and its associated calculational scheme[18]. Before starting discussing the key points of DFT, let us recall that, owing to the one- and two-particle nature of the operator of the Hamiltonian, the total energy of any many-body wave function can be written in terms of the generalized one- and two-electron densities and that, in the case of the HF method, the generalized one-electron density is sufficient.

Although the Hohenberg–Kohn theorem is established as the fundamental theorem of quantum chemistry based on electron density, it is not in itself sufficient to calculate actual electronic motion states. In the next year, Kohn and Sham developed an electronic state calculation method derived from this theorem, which is called the Kohn–Sham method[39]. The Kohn–Sham method is a variational approach using the electron-electron interaction potential of the density functional to give the lowest (ground state) energy and the corresponding molecular orbitals and orbital energies[39]. From a practical viewpoint, the most significant characteristic of this method is the use of the independent-electron approximation for kinetic energy, similarly to the Hartree–Fock method, instead of the kinetic energy functional in the Thomas–Fermi method[39]. This simple replacement solved the weakest point of the Thomas–Fermi method. So, the Kohn–Sham method, using the independent-electron kinetic energy, made it possible to carry out highspeed quantitative electronic structure calculations in chemistry and solid-state physics through the development of sophisticated exchange-correlation functionals. This has led to an explosion in the use of DFT[39]. Note, however, that, the Kohn–Sham method is not a pure DFT in the spirit of the Thomas–Fermi method. Nevertheless, it should be emphasized that the Kohn–Sham method is an exact formulation of the Hohenberg–Kohn[41] theorem in the sense that electronic structures are determined using the one-to-one correspondence between external potential and electron density on the basis of the variational principle.

II.6.1. The first Hohenberg-Kohn theorem

The first Hohenberg-Kohn theorem (Hohenberg and Kohn 1964, [39]) legitimizes the use of electron density $\rho(r)$ as a basic variable. It states: “The external potential v(r) is determined, within a trivial

additive constant, by the electron density ρ(r)." Since ρ(r) determines the number of electrons, it follows that ρ(r) also determines the ground-state wave function and all other electronic properties of the system. Note that v(r) is not restricted to Coulomb potentials[42]. Owing to the 1st H-K theorem, the energy is expressed under the form of a functional of the electron density:

$$E_v[\rho(r)] = T[\rho(r)] + V_{ne}[\rho(r)] + V_{ee}[\rho(r)] \qquad (20)$$

V_{ee} contains the classical Coulomb repulsion term and a non-classical term so the energy can be decomposed into terms depending on the external potential and a universal function, the Hohenberg and Kohn functional, F_{HK}:

$$E_v[\rho(r)] = T[\rho(r)] + V_{ne}[\rho(r)] + J[\rho(r)] + \text{non} - \text{classical term}$$

$$= \int \rho(r)v(r)\,dr + F_{HK}[\rho(r)] \qquad (21)$$

where $J[\rho(r)]$ is the classical Coulomb repulsion. The non-classical term is a very elusive, very important quantity; it is the major part of the "exchange-correlation energy[42].

II.6.2. The Second Hohenberg-Kohn theorem

The second Hohenberg-Kohn theorem (Hohenberg and Kohn 1964) provides[18] the energy variational principle. It reads: "for a trial density $\rho'(r)$ such that $\rho'(r) \geq 0$ at any r and $\int \rho'(r)dr = N$, the electron density obeys a variational principle:[42]

$$E_v[(\rho'(r))] \geq E_0 \qquad (22)$$

where $E_v[(\rho'(r)]$ is the energy functional and E_0 is the true ground state energy. Consequently, the exact density gives E_0, the electronic ground state energy. Then, among approximate energies, the best one is the one that gives the lowest energy, and solution can be obtained by minimizing the energy within the constraint that the electron density integrates to N[18]. Therefore, assuming differentiability of $E_v[\rho(r)]$, this variation principle requires that the ground state density satisfied the following stationary principle:

$$\delta\{E_v[\rho(r) - \mu[\int \rho(r) - N]\} = 0 \qquad (23)$$

which gives the Euler-Lagrange equation:

$$\mu = \frac{\delta E_v[\rho(r)]}{\delta\rho(r)} = v(r) + \frac{\delta F_{HK}[\rho(r)]}{\delta\rho(r)} \qquad (24)$$

If we knew the exact $F_{HK}[\rho(r)$, it would be an exact equation for the ground-state electron density. Note that $F_{HK}[\rho(r)$ is defined independently of the external potential $v(r)$. This means that $F_{HK}[\rho(r)$ is a universal functional of $\rho(r)$. Once we have an explicit form (approximate or accurate) for $F_{HK}[\rho(r)$, we can apply this method to any system. Eq. 24 is the basic working equation of

Hohenberg-Kohn density functional theory[42]. Still, this approach presents limitations when searching for improved F_{HK} functionals, and more precisely their kinetic energy and non-classical parts.

II.6.3. The Kohn-Sham method

In their model[43], Kohn and Sham considered a fictitious system of N interacting electrons moving in an effective field V_{eff}. This system is completely described by a Slater determinant whose spin-orbitals $\Theta_i(x) = \phi_i(r)\,\sigma_i(\omega)$, called Kohn-Sham spin-orbitals (and ϕ_i, the Kohn-Sham orbitals), can be determined - by analogy to the Hartree-Fock method - using the equation:

$$\hat{h}^{KS}\phi_i = \varepsilon_i\phi_i \quad (25)$$

where $\hat{h}^{KS}$ defines the monoelectronic (mean-field) Kohn-Sham operator:

$$\hat{h}^{KS} = -\frac{1}{2}\nabla^2 + \hat{V}_{eff}(\vec{r}) \quad (26)$$

The relation between this fictitious system and the real one is established in the choice of the effective potential, which is made in such a way that the density calculated from the square of the modulus of the orbitals ϕ_i is equal to that of the real system of interacting electrons:

$$\rho_s(\vec{r}) = \sum_i^N |\Theta_i|^2 = \rho_0(\vec{r}) \quad (27)$$

Considering non-interacting electrons enables in fact to evaluate easily the kinetic energy, $T_s[\rho(\vec{r})]$

$$T_s[\rho(\vec{r})] = -\frac{1}{2}\sum_i^N \langle\Theta_i|\nabla^2|\Theta_i\rangle \quad (28)$$

The expression of the total energy of the interacting system then becomes:

$$E[\rho(\vec{r})] = T_s[\rho(\vec{r})] + J[\rho(\vec{r})] + E_{XC}[\rho(\vec{r})] + E_{Ne}[\rho(\vec{r})] \quad (29)$$

where $E_{XC}[\rho(\vec{r})]$ is the exchange-correlation energy which contains in addition to the unclassical contributions $E_{ncl}[\rho(\vec{r})]$ the part of the kinetic energy not described by the fictitious system and which depends on electron-electron interactions: $T_c[\rho(\vec{r})] = T[\rho(\vec{r})] - T_s[\rho(\vec{r})]$. Now, by applying the variational principle we arrive at the following expression for the effective potential:

$$V_{eff}(\vec{r}) = \int \frac{\rho(\vec{r}\prime)}{|\vec{r}-\vec{r}\prime|}d\vec{r}' + V_{XC}(\vec{r}) - \sum_A^M \frac{Z_A}{|\vec{r}-\vec{r}_A|} \quad (30)$$

with

$$V_{XC}(\vec{r}) = \frac{\partial E_{XC}[\rho(\vec{r})]}{\partial\rho(\vec{r})} \quad (31)$$

Note that due to the fact that ρ occurs from the start in the potential V_{eff}, the KS equation has to be solved in an iterative way, just like the HF equations. Still, the problem is not that simple since in Eq.(31) the different terms are not all known. Indeed, as we do not know the exact expression of the exchange-correlation energy E_{XC}, we have no indication of the explicit form of the potential V_{XC}, which corresponds to it.

II.6.4: Exchange-Correlation Functionals

In the previous section, the fundamentals of the Kohn–Sham method and its derivative theories have been explained without referring to the specific forms of exchange-correlation functionals used. The Kohn–Sham method is an established quantum theory based not only on electron density but also on a rigorous exchange-correlation functional. It is therefore difficult to assess the reliability of the Kohn–Sham method and its derivative theories without specifically considering the exchange-correlation functional used[40]. In this section, we examine the exchange-correlation functionals that have been developed so far, with their features and problems. In particular we concentrate on those XC functionals that were used in this work. The exchange-correlation functional is the only part that is approximated in the Kohn–Sham equation. Therefore, the reliability of the Kohn–Sham method depends on the validity of this approximated functional[40].

A variety of exchange-correlation functionals have thus far been developed on the basis of different physical models. The XC functionals are classified based on their characteristics. These standard functionals are often arranged hierarchically, as in Jacob's ladder shown in Fig. II.1.

The first general approximation for exchange and correlation was the **local density approximation (LDA)**, *i.e.* the XC functional depends only on the electron density ρ(r). It assumes that the XC energy of a non-uniform system can be obtained by applying uniform electron-gas results for infinitesimal portions of the non-uniform electron distribution[39].

Generalized gradient approximation (GGA): These functionals depend on both density and its density gradient $\nabla\rho$. GGA functionals achieve good ground state energies, improve significantly the dissociation energies and bond lengths, reproduce more accurately the cohesive properties of solids, and correct the vibrational frequencies of molecules[39].

Meta-GGA functionals: these functionals correct the GGA functionals with a dependence on the kinetic energy density τ(r). Several properties are improved with respect to GGA functionals such as the atomic energies, H-bond dissociation energies, and lattice constants[39].

Hybrid functionals: At the beginning of the 90s, Becke proposed to introduce a percentage of exact Hartree–Fock exchange in the XC functionals (in fact the exchange part). Contrary to LDA and GGA exchanges, which are local, HF exchange is non-local and present the exact $\frac{-1}{r}$ asymptotic behavior. This $\frac{-1}{r}$ asymptotic behavior can exactly compensate the $\frac{1}{r}$ Coulomb repulsion term, canceling out any self-interaction, like in a HF treatment. For describing HF exchange, the X functional depends on the occupied MOs.

The fifth rung concerns **Double Hybrids** where, in addition to a percentage of HF exchange included in the exchange functional, a given percentage of MP2 correlation is added to the correlation functional. In this case, the functional depends on the occupied and unoccupied MOs. Of course, these functionals do not present the advantage of including electron correlation at the computational cost of HF calculations. Still, they find an interest to provide improved thermodynamical properties.

Note that besides the double hybrids, the XC functionals are not suited for evaluating the London dispersion forces, which is required for describing van der Waals interactions and the balance between electrostatic, exchange-repulsion, and dispersion effects. Still, empirical expressions have been proposed to describe the London dispersion forces, like in the ωB97X-D XC functional.

Table II.1 lists the exchange-correlation functionals employed in this work and emphasizes to which rung they belong. In addition, the amount of HF exchange is given as well as, for double hybrids, the amount of MP2 correlation. Note that for range-separated hybrids, the % of HF exchange at short-range (r = 0) and long-range (r = ∞) are given as well as the value of the range-separating parameter (ω).

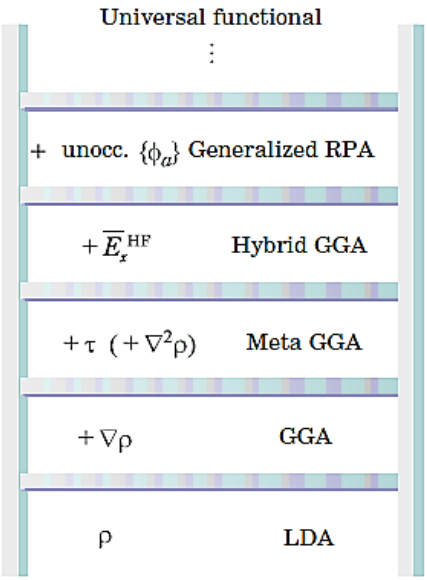

Fig.II.1: Jacob's ladder in the development of functional[39].

Table II.1 List of exchange-correlation functionals used in this work.

Type of functional	XC Functional	% of HF exchange (short-range, long-range)
LDA	SVWN	0, 0
GGA	BLYP	0, 0
mGGA	TPSS	0, 0
Global hybrids	B3LYP M06 M05	20, 20 27, 27 28, 28
Ranged-separated hybrids	ωB97 ωB97X ωB97X-D	0, 100 (ω = 0.4 $bohr^{-1}$) 16, 100 (ω = 0.3 $bohr^{-1}$) 22, 100 (ω = 0.2 $bohr^{-1}$)
Double hybrids	B2PLYP	53, 53 HF exchange 27 MP2 correlation

II.7. The polarizable continuum model and solute-shaped cavities

Effects of solvents on spectroscopic, structural and electronic properties are topics of great interest in current physical chemistry. We expose in this section the main ideas behind continuous models, their advantages and limitations. Unlike the solid phase, where there is a large order, and the gas phase, for which we can neglect intermolecular interactions, there is still no model for an ideal liquid because it is dense and disordered. We can represent a liquid considering explicit solvation, that is, by including many solvent molecules in the calculations as well as by accounting for their dynamics. However, this treatment may be computationally difficult and several proposals for approximations have emerged to represent the liquid, aiming at a balance between a good description and cost computational[44]. Within this perspective the methods called Continuous Models with Kirkwood[45], Onsager [46],Tapia and Goscinski[47], and Rivail and Rinaldi[48] have emerged. They are based on inserting the solute into a spherical cavity in a continuous medium represented by its dielectric constant. Fig.II.2 the distribution of molecular charges generates a dipole moment ($\boldsymbol{\mu}$), this dipole polarizes the dielectric medium that generates a reaction field that will change the distribution of charges in the molecule and thus creates a self-consistent reaction field (SCRF) cycle that polarizes the solute. Other implementations consider the contribution of the other polarization moments such as quadrupoles, octopoles, etc. [49]

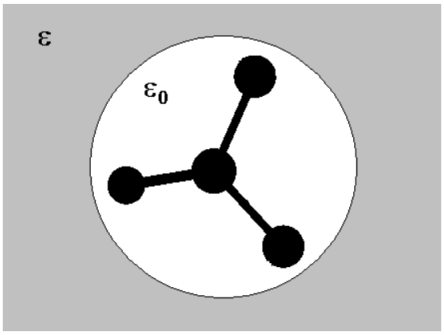

Fig.II.2. Solute in a spherical cavity immersed in a continuum described by it constant dielectric[44].

Many models have emerged based on this theory and today the one that stands out the most is the Polarizable Continuum Model (PCM - Polarizable Continuum Model)[50]. In PCM, the cavity is not spherical anymore. It is built from the overlap of spheres centered on the atoms of the molecule, where the radius of these spheres is typically 20% greater than the atomic van der Waals radii. This results in a cavity having the same shape as the molecule. Then, owing to the molecular shape, there might be zones inaccessible to the solvent molecules so that a solvent excluded surface can be obtained by circulating a (spherical) solvent molecule around the cavity. This surface, also called the Connally molecular surface, defines the topological boundary of the union of the solvent probes that do not overlap with the molecule. In addition to this improvement, PCM treats electrostatic interactions through a surface charge density on the surface cavity (Fig.II.3)[44]. This gives rise to the apparent surface charge (ASC) and the convenient integral equation formalism (IEF).

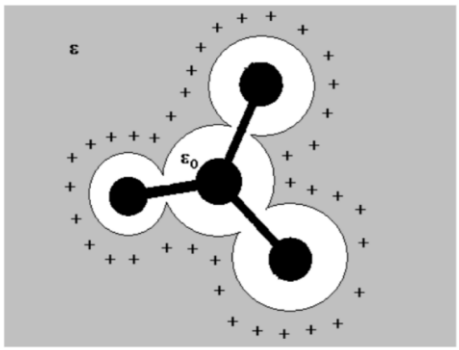

Fig.II.3. The PCM model[44].

The charge distribution of the solute, inside the cavity, polarizes the dielectric continuum, which in return polarizes the solute charge distribution. Evaluating the solute-solvent interactions corresponds therefore to a self-consistent process that is solved numerically following an iterative procedure. In that procedure, the solute-solvent interaction term is added to the Hamiltonian. Here we just give the expression of the apparent surface charge, highlighting its dependence on the dielectric constant of the solvent:

$$\sigma(\vec{s}) = \frac{\varepsilon-1}{4\pi\varepsilon}\vec{E}_{SCRF}.\vec{n} \qquad (32)$$

where $\vec{s}$ is a position vector on the surface and $\vec{n}$ is a unitary vector perpendicular to the outside surface of the cavity. In practice this surface is approximated in terms of a set of finite elements

(called tesserae). This model has been widely used and has been successful. One of its advantages is that additional electrons are not included in quantum calculations. In general, this approach is reliable for polar molecular systems but less when there are specific solute-solvent interactions, as hydrogen bonds [43].

II.8. Structure optimization strategy and evaluation of the thermodynamical state functions.

One of the most essential tasks in theoretical chemistry is geometry optimization. Since energy evaluations can be quite costly, depending on the chosen electronic structure method we have to reduce as much as possible the number of structures to probe on the potential energy surface (PES). Most geometry optimizers are based on the gradient: the gradient gives a good first estimate of the direction in which one can find, for example, a minimum. So, each optimization step occurs as follows: the gradients (first-order derivatives) of the energy are evaluated with respect to the atomic Cartesian coordinates of each atom. Regarding the optimization method (convergence parameters, …) or kind of element of geometry that we want to treat, geometry optimization scheme in Gaussian can be highly tuned[51,52]. Selecting a new geometry is done by sophisticated algorithms, aiming for rapid convergence to the geometry of the lowest energy. At the end, at minimum energy geometry the force on each atom is zero. It is important to recognize that this procedure will not necessarily find the global minimum, i.e. the geometry with the lowest energy. Naturally, a search for a minimum finds a local minimum but not necessarily the lowest, i.e. the global minimum. This means that different regions of the PES should be probed (like in this work to locate the different rotamers). In fact, the optimization procedure stops when it finds a stationary point, i.e. a point where forces (or gradients) on the atoms are zero, and this may be also a saddle point (*i.e.* a transition state structure). Nevertheless, by performing vibrational frequencies calculations second-order derivatives are calculated. Then, the positive signal of the frequencies (all frequencies should be real) ensures that the geometry is a minimum and not a saddle point[51,52].

The equations used for computing thermochemical data in Gaussian are equivalent to those given in standard texts on thermodynamics. Much of what is discussed below is covered in detail in "Molecular Thermodynamics" by McQuarrie and Simon (1999)[53]. The starting point in each case is the evaluation of the partition function, $q(V,T)$. The partition function can be used to determine the thermodynamical state functions, like the entropy S:

$$S = k_B \, ln[q(V,T)] + k_B T \left(\frac{\partial lnq}{\partial T}\right)_V \qquad (33)$$

where k_B is Boltzmann constant ($k_B = 1.380662\ 10^{-23}$ J/K, corresponding to the gas constant divided by the Avogadro's number) and T is the temperature. Assuming independent contributions of the translational, rotational, vibrational, and electronic partition functions the entropy can be expressed as

$$q = q_t q_e q_r q_v \qquad (34)$$

III. MOTIVATIONS AND OBJECTIVES

For this investigation, we have selected a set of nine N-salicylideneaniline derivatives (Scheme 2). These compounds are based on the reference (E)-2-methoxy-6-(pyridine-3-yliminomethyl)phenol compound (1), usually referred to as PYV3[54]. These compounds differ by the number (1 or 2) and positions of the N atoms of the "aniline" ring. In this master thesis, by using quantum chemistry calculations, we investigate the thermodynamics of these condensation reactions. This is performed at several levels of approximation in order to assess the impact of electron correlation. In particular, after defining high-level reference values, density functional theory (DFT) calculations are performed and the performance of exchange-correlation (XC) functionals is assessed.

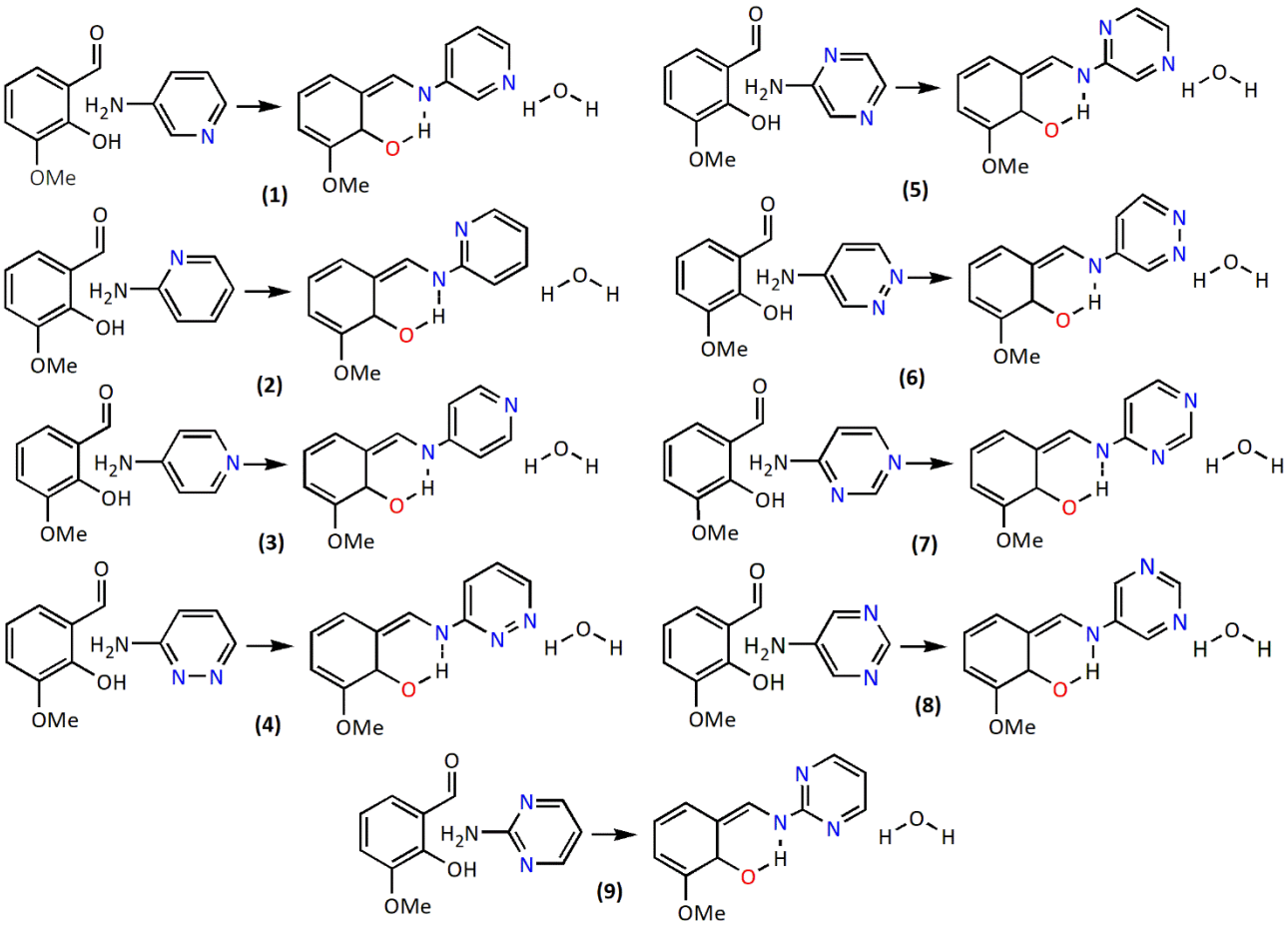

Scheme 2. List of the selected N-salicylideneaniline derivatives (in their OH form) as well as the corresponding condensation reactions.

IV. RESULTS AND DISCUSSION

IV. 1. Geometry Optimizations

Molecular geometry is at the roots of the properties of a substance including its reactivity, its polarity, its phases of matter (as a function of temperature), its color, its electric and magnetic properties, its thermodynamics, as well as its biological activity or performance as a smart material. In order to predict the geometrical structures of the anil derivatives, MP2/cc-pVTZ geometry optimizations were carried out using the Gaussian 16 package[52], i) for the isolated molecules (corresponding to an infinite diluted gas phase) and ii) for the molecules in solution, by using the polarizable continuum model (PCM). Dichloromethane (CH_2Cl_2) was used as solvent. We have considered the *cis*-enol (OH form) and *cis*-keto (NH form) species. The *trans*-keto form has not been considered because the absence of H-bond leads to higher energy. Still, as a function of the position of the N atom(s) in the ring, one or two conformers (rotamers) correspond to minima on the potential energy surface. They have been both considered as well as their relative energies. Remarkable bond lengths and torsion angles of the 9 *N*-salicylideneaniline derivatives are listed in table IV.1 (OH form) and IV.2 (NH form).

IV.1.1. Geometry Optimization of the Enol Form

As shown in Table IV.1 the position of the N atom of the pyridine (compounds **1**, **2**, and **3**) or of the N atoms of the pyridazine (**4**), pyrazine (**5** and **6**), and pyrimidine (**7**, **8**, and **9**) has a small impact on the geometry of the rest of the molecule and particularly the molecular fragment involving the enol-imine functions. On the other hand, larger differences appear for the dihedral angle describing the torsion between the imine function and the nitrogenated aromatic ring (T_1). Similar results are obtained for the isolated molecule as well as for the molecule in CH_2Cl_2, as treated with PCM. The presence of the solvent increases the O-C3 bond length, decreases the C3=C4 one, increases the C4-C7, decreases the C7=N, which corresponds to an increase enol character. At the same time the H-bond is strengthened (the N-H bond length decreases). Differences of energies between the conformers of rotation are either very small (< 0.5 kcal/mol) or of the order of 3 kcal/mol (2 kcal/mol) for the isolated (solvated) species. Though we come back later on the discussion of the condensation energies, Fig.IV.1. looks for a possible relationship between the ΔE^0 of condensation and T_1. No systematic trend could be unraveled.

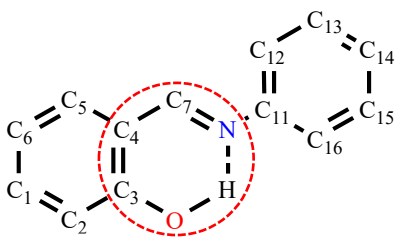

Scheme 3. Atom numbering used for describing the geometries of the enol species. For simplicity, most of H atoms are not drawn while the N atoms of the pyridines/diazines are replaced by C atoms.

Table IV.1 Remarkable bond lengths (Å) and torsion angles (degrees) of the nine enol derivatives, as obtained from geometry optimization at the MP2/cc-pVTZ level, either for the isolated molecule (diluted gas phase) or by accounting for solvent (CH_2Cl_2) effects using the IEFPCM method. The ΔE^0 of condensation (kcal/mol) are also given as well as their differences for isomers with two different rotamers.

Bonds	1		**2**		**3**	**4**		**5**		**6**		**7**		**8**	**9**
	15=N	13=N	12=N	16=N	14=N	15,16=N	12,13=N	12,15=N	13,16=N	14,15=N	13,14=N	14,16=N	12,14=N	13,15=N	12,16=N
Isolated molecules															
H-O	0.994	0.993	0.997	0.994	0.993	0.993	0.993	0.994	0.992	0.991	0.997	0.992	0.994	0.991	0.997
O-C3	1.343	1.343	1.343	1.341	1.343	1.341	1.343	1.342	1.341	1.343	1.343	1.342	1.342	1.343	1.340
C3-C4	1.413	1.412	1.413	1.412	1.412	1.413	1.412	1.413	1.413	1.413	1.412	1.413	1.413	1.413	1.414
C4-C7	1.444	1.443	1.444	1.444	1.444	1.443	1.442	1.441	1.445	1.442	1.442	1.443	1.441	1.442	1.442
C7-N	1.295	1.295	1.295	1.292	1.294	1.294	1.296	1.297	1.294	1.295	1.295	1.293	1.296	1.297	1.294
N-H	1.710	1.709	1.702	1.705	1.712	1.715	1.704	1.701	1.715	1.725	1.724	1.719	1.701	1.720	1.688
T_1	38.8	42.0	12.4	42.6	42.9	42.9	32.7	9.6	42.5	42.0	43.0	46.2	24.0	41.1	16.4
ΔE^0	-13.5	**-13.8**	**-12.7**	-9.5	**-11.9**	-8.3	**-11.7**	**-12.7**	-9.7	-10.9	**-11.1**	-6.8	**-9.8**	**-12.8**	**-7.2**
$\Delta\Delta E^0$	+0.3			3.2		3.4			3.0	0.2		3.0			
CH_2Cl_2															
H-O	0.997	0.996	0.999	0.996	0.996	0.995	0.995	0.997	0.995	0.993	0.993	0.994	0.996	0.994	0.999
O-C3	1.345	1.345	1.346	1.345	1.345	1.345	1.345	1.345	1.345	1.345	1.345	1.345	1.344	1.345	1.344
C3-C4	1.412	1.411	1.412	1.411	1.412	1.412	1.412	1.413	1.412	1.413	1.411	1.412	1.412	1.412	1.413
C4-C7	1.446	1.446	1.445	1.445	1.445	1.445	1.444	1.444	1.445	1.444	1.444	1.445	1.443	1.444	1.445
C7-N	1.295	1.294	1.293	1.292	1.293	1.293	1.294	1.295	1.294	1.295	1.294	1.293	1.294	1.296	1.293
N-H	1.694	1.696	1.679	1.694	1.700	1.701	1.698	1.692	1.703	1.713	1.713	1.706	1.695	1.708	1.682
T_1	37.0	42.3	18.1	40.0	40.3	40.3	26.9	16.1	43.9	40.9	43.2	43.8	16.6	40.4	23.2
ΔE^0	**-12.5**	**-12.5**	-11.7	**-12.0**	**-10.4**	-8.3	**-10.0**	**-11.2**	-9.3	**-9.0**	**-9.0**	-6.2	**-7.9**	**-11.2**	**-7.3**
$\Delta\Delta E^0$			0.3			1.7			1.9			1.7			

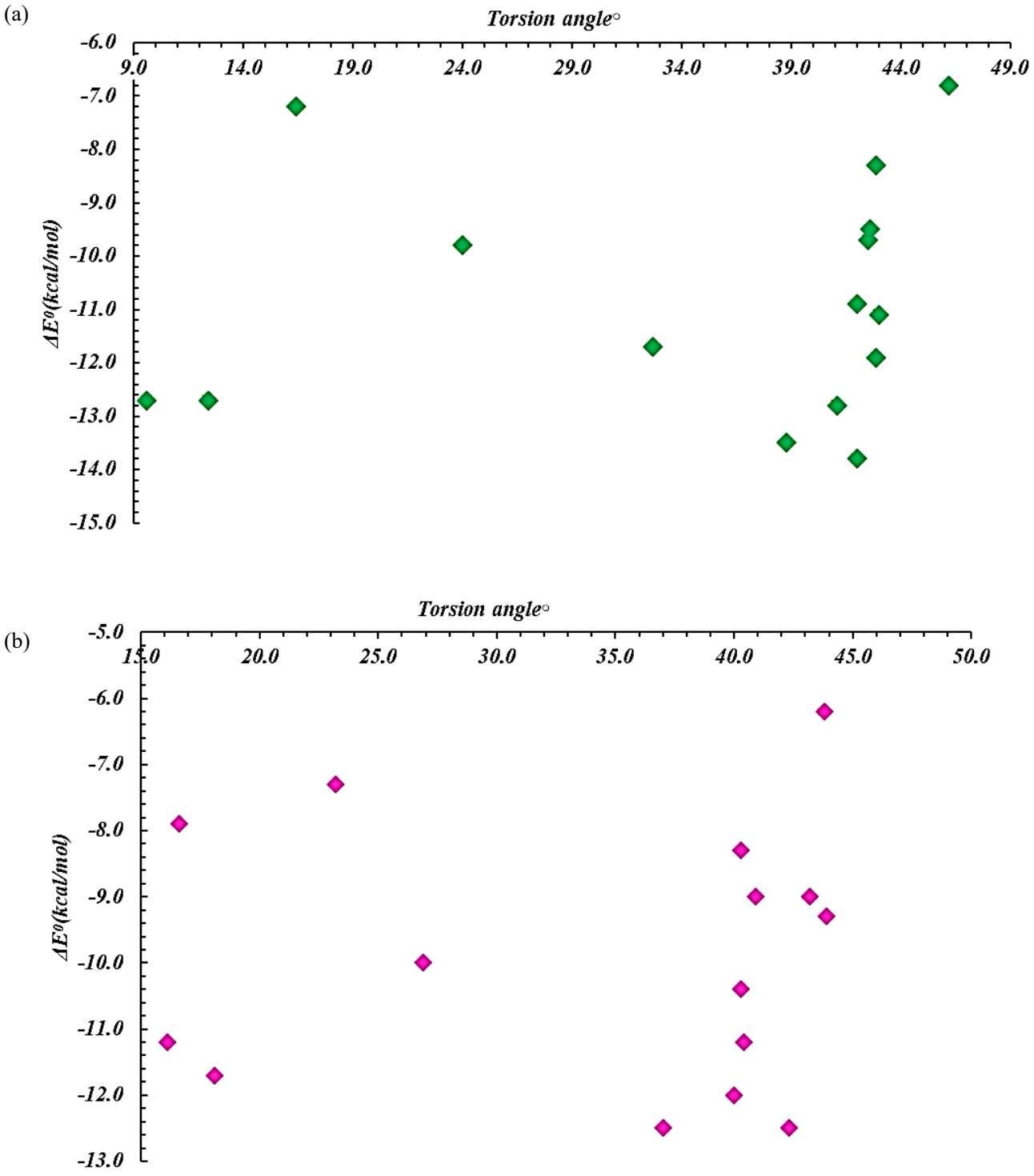

Fig. IV.1: ΔE^0 values of the condensation reactions to get the enol species as a function of the torsion angles in degrees. (a) isolated molecules (b) in CH_2Cl_2 (IEFPCM). All calculations were performed at the MP2/cc-pVTZ level of approximation.

IV.1.2. Geometry Optimization of Keto Form

Contrary to the case of the enol form discussed in the previous paragraph, the nature of the ring linked to the nitrogen of the enamine has a stronger impact on the geometry of the keto-enamine ring (Table IV.2). This effect is particularly important on the H-bond length (d_{NH}). On the other hand, the solvent effects lead to the same trends: the O=C3 and C4=C7 bonds (having a double bond character) are lengthened while the C3-C4 and C7-N bonds (having a single bond character) are shortened. Again, this corresponds to an increase enol character or rather a reduction of the keto character. In gas phase, the differences of energies between the rotamers are similar to what has been observed for the enol forms and, again, these differences are reduced when solvent effects are taken into account. A noticeable difference between the keto and enol forms is the reduced torsion angle (T_1) values for the keto ones. So, the keto tautomers are more planar than the enol ones. On the other hand, as shown in Fig.IV.2 there is again no relationship between the energies of condensation and the amplitude of this torsion angle.

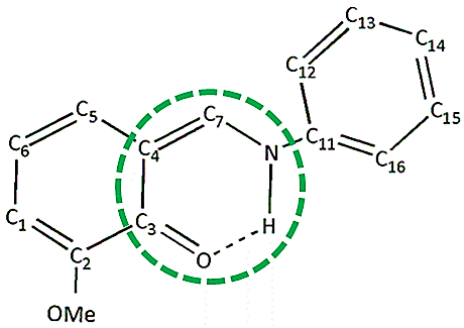

Scheme 4. Atom numbering used for describing the geometries of the keto species. For simplicity, most of H atoms are not drawn while the N atoms of the pyridines/diazines are replaced by C atoms.

Table IV.2 Remarkable bond lengths (Å) and torsion angles (degrees) of the nine keto derivatives, as obtained from geometry optimization at the MP2/cc-pVTZ level, either for the isolated molecule (diluted gas phase) or by accounting for solvent (CH_2Cl_2) effects using the IEFPCM method The ΔE^0 of condensation (kcal/mol) are also given as well as their differences for isomers with two different rotamers.

Bonds	1		**2**		**3**	**4**		**5**		**6**		**7**		**8**	**9**
	15=N	13=N	12=N	16=N	14=N	15,16=N	12,13=N	12,15=N	13,16=N	14,15=N	13,14=N	14,16=N	12,14=N	13,15=N	12,16=N
Isolated molecules															
H-O	1.534	1.610	1.524	1.620	1.521	1.622	1.509	1.514	1.604	1.516	1.623	1.652	1.568	1.654	1.656
O-C3	1.261	1.263	1.275	1.265	1.276	1.263	1.275	1.274	1.265	1.272	1.268	1.261	1.269	1.261	1.262
C3-C4	1.451	1.452	1.450	1.455	1.450	1.458	1.452	1.452	1.457	1.454	1.452	1.457	1.456	1.452	1.459
C4-C7	1.393	1.394	1.398	1.393	1.398	1.389	1.395	1.395	1.390	1.393	1.391	1.387	1.391	1.441	1.388
C7-N	1.329	1.326	1.321	1.325	1.321	1.329	1.326	1.326	1.329	1.327	1.325	1.332	1.331	1.330	1.331
N-H	1.071	1.055	1.070	1.052	1.079	1.052	1.074	1.073	1.054	1.073	1.053	1.073	1.058	1.073	1.043
T_1	10.3	14.3	0.8	10.1	15.2	4.4	1.4	0.5	10.6	8.5	8.9	0.6	0.6	6.8	0.3
ΔE^0	*-6.2*	*-6.0*	-5.8	*-2.2*	-3.5	-0.4	-2.1	-5.0	-1.6	-2.0	-1.6	-0.5	-3.0	-7.80	-9.76
$\Delta\Delta E^0$		*0.2*		*3.6*		*1.7*			*3.4*		*0.4*	*2.5*			
CH_2Cl_2															
H-O	1.561	1.606	1.568	1.610	1.553	1.604	1.601	1.656	1.651	1.656	1.652	1.641	1.652	1.645	1.649
O-C3	1.283	1.275	1.278	1.273	1.277	1.271	1.276	1.275	1.272	1.275	1.270	1.268	1.271	1.273	1.269
C3-C4	1.440	1.441	1.447	1.449	1.447	1.451	1.448	1.450	1.450	1.450	1.436	1.454	1.452	1.451	1.454
C4-C7	1.407	1.406	1.405	1.402	1.403	1.497	1.499	1.496	1.497	1.496	1.491	1.494	1.495	1.493	1.495
C7-N	1.315	1.315	1.316	1.316	1.318	1.322	1.321	1.327	1.322	1.327	1.324	1.325	1.324	1.321	1.322
N-H	1.063	1.054	1.061	1.053	1.065	1.050	1.061	1.063	1.056	1.065	1.059	1.057	1.052	1.068	1.050
T_1	14.7	19.1	1.2	7.7	13.6	5.8	2.0	0.7	7.5	7.8	8.0	1.2	0.3	14.2	0.5
ΔE^0	-7.0	-6.3	*-6.1*	-3.9	-3.5	-1.7	-3.4	-4.7	*-2.4*	-1.4	-1.1	*-0.2*	-2.08	-11.5	-2.12
$\Delta\Delta E^0$		0.9		2.2		*1.7*			*2.3*		0.3	*1.8*			

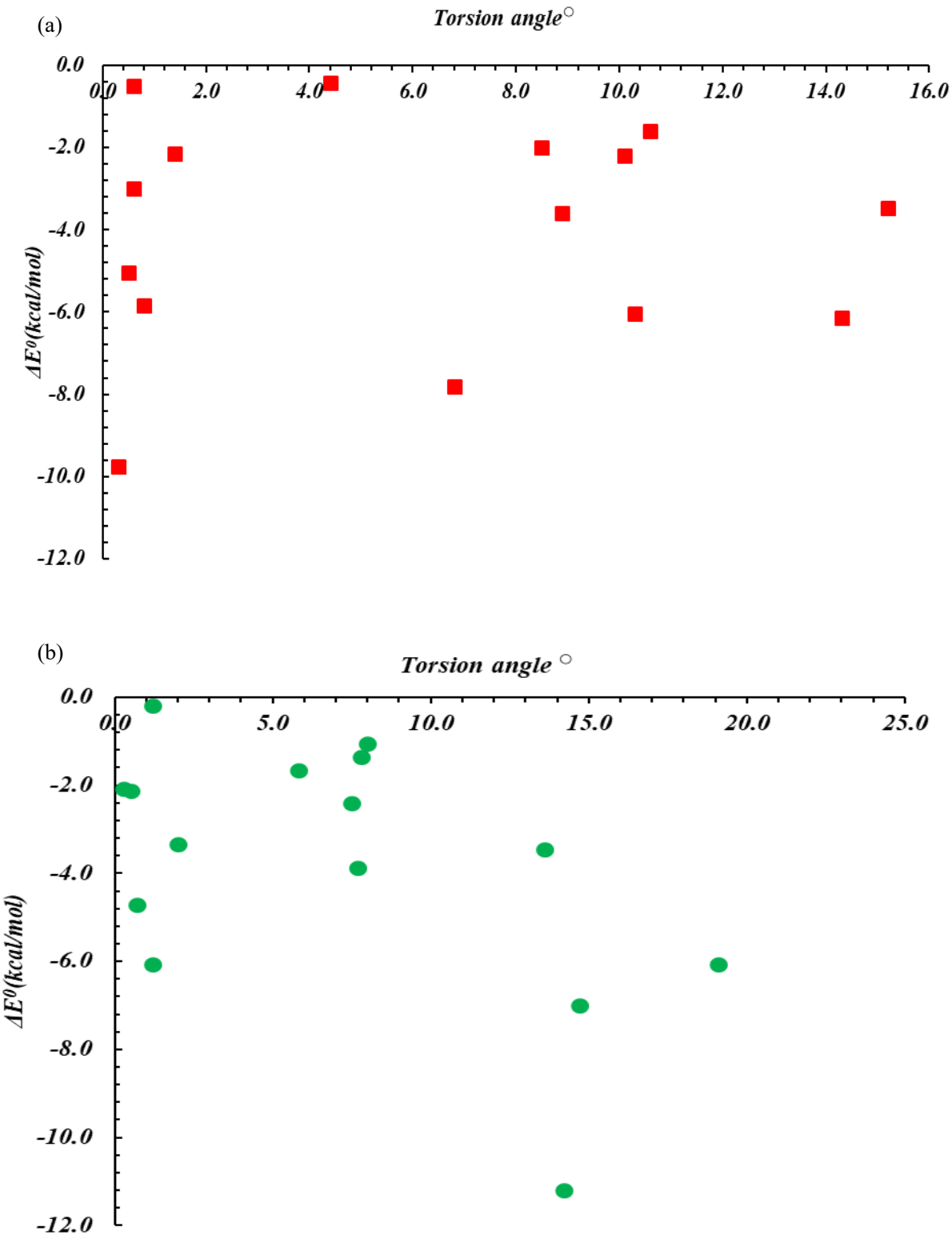

Fig.IV.2: ΔE^0 values of the condensation reactions to get the keto species as a function of the torsion angles in degrees. (a) isolated molecules (b) in CH_2Cl_2 (IEFPCM). All calculations were performed at the MP2/cc-pVTZ level of approximation.

IV. 2. Thermodynamics of the condensation reactions with wavefunction methods

IV.2.1. MP2 results

Based on the MP2 optimized geometries, the thermodynamics of the condensation reactions to prepare the anil derivatives has been studied. The targets are the energies of these reactions of condensation: the electronic energies (ΔE, which corresponds to a 0K energy without the zeron-point vibrational energy) as well as the internal energies ΔU_0^0, the enthalpies (ΔH^0), and the Gibbs free energies (ΔG^0) at 298.15 K. The internal energies differ from the electronic energies by the addition of the zero-point vibrational energy contributions. Then, the enthalpies add to the internal energies the thermal contributions while entropic contributions are included to get the Gibbs free energies. These calculations were performed in gas phase and in CH_2Cl_2. All vibrational frequencies are real for all species, demonstrating that these geometries are minima on the potential energy surface. All these calculations were performed using Gaussian 16 package[52]

These condensation energies were evaluated at different levels of approximation: first, using wavefunction methods to investigate the effects of adding the successive contributions of electron correlation and then, using density functional theory to assess the performance of XC functionals and then to select the most promising (Section IV.3).

The wavefunction methods include: the reference Hartree-Fock method, second (MP2), third (MP3), and fourth (MP4) orders Møller-Plesset perturbation theory, configuration interactions methods with doubles (CID) as well as with singles and doubles (CISD), and finally coupled cluster methods with doubles (CCD) as well as with singles and doubles (CCSD). The highest-level quantities are obtained at the CCSD level, which will be used as reference. Note that CID and CISD are not size-consistent methods so that the size-consistent corrected schemes of Davidson have also been considered. At these levels of approximation, we used the MP2 optimized geometries and therefore we only considered the electronic energies (in gas phase and in CH_2Cl_2).

Tables IV.3 and IV.4 present the MP2/cc-pVTZ results in gas phase and in CH_2Cl_2 (IEF-PCM) for the condensation reaction leading to the formation of the enol tautomer. To analyze the results, let us first consider two groups of compounds: group 1 with one N atom on the amine (compounds **1**, **2**, and **3**) and group 2 with two N atoms on the amine (compounds **4**, **5**, **6**, **7**, **8** and **9**). It is noteworthy that for group 1, the "energies"[1] of formation are the most negative for compound **1** (N in position 3), *i.e.* the condensation reaction is the most exothermic (ΔH^0) and exergonic (ΔG^0). It is followed by compound **2** (N in position 2) and compound **3** (N in position 4). In the case of group 2, the most negative values are also obtained when at least one N atom is in position 3 with respect to the C atom of the imine. So, compound **8** with N atoms in 3 and 3'(5) positions have the lowest "energies" of formation, except for ΔG^0 where it is compound **5** (N in position 2 and 3' (5)). So, in summary, for the enthalpies:

Group 1: **1** (N in position 3) < **2** (2) < **3** (4)

Group 2: **8** (3, 3') < **5** (2, 3') < **6** (3, 4) < **4** (2, 3) < **9** (2, 2') < **7** (2, 4)

[1] The compact "energies" notation was employed to encompass the different types of energies discussed above.

Table IV.3. Thermodynamic values (kcal/mol) of the condensation reactions to form the enol tautomer as calculated at the **MP2/CC-pVTZ** level of approximation in gas phase. In parentheses are given the results for the other rotamers when their energy of condensation is smaller. Due to lack of time the other thermodynamic values are not yet available.

Compounds	**ΔE^0**	**ΔU_0^0**	**ΔH^0**	**ΔG^0**
1	-13.5 (-13.8)	-14.0	-13.9	-11.4
2	-12.7	-13.2	-13.2	-11.2
3	-11.9	-12.4	-12.4	-10.0
4	-8.3 (-11.7)	-8.9	-8.9	-6.5
5	-12.7	-12.4	-12.4	-10.7
6	-10.9 (-11.1)	-11.4	-11.4	-9.0
7	-6.8 (-9.8)	-7.4	-7.4	-5.1
8	-12.8	-13.2	-13.2	-10.6
9	-7.2	-7.8	-7.8	-5.7

Table IV.4. Thermodynamic values (kcal/mol) of the condensation reactions to form the enol tautomer as calculated at the **MP2/CC-pVTZ** level of approximation in **CH_2Cl_2.** In parentheses are given the results for the other rotamers when their energy of condensation is smaller. Due to lack of time the other thermodynamic values are not yet available.

Compounds	**ΔE^0**	**ΔU_0^0**	**ΔH^0**	**ΔG^0**
1	-12.5	-13.2	-13.2	-10.6
2	-11.7 (-12.0)	-12.4	-12.4	-10.2
3	-10.4	-11.2	-11.2	-8.8
4	-8.3 (-10.0)	-9.0	-9.0	-6.5
5	-11.2	-11.2	-11.1	-9.1
6	-9.0	-9.7	-9.7	-7.2
7	-6.2 (-7.9)	-7.0	-6.9	-4.5
8	-11.2	-11.9	-11.9	-9.3
9	-7.3	-8.0	-8.0	-5.7

The same orderings are observed when the calculations account for solvent effects, though the amplitudes of the "energies" are usually smaller.

Group 1: **1** (N in position 3) < **2** (2) < **3** (4)

Group 2: **8** (3, 3') < **5** (2, 3') < **6** (3, 4) < **4** (2, 3) < **9** (2, 2') < **7** (2, 4)

Figure. IV.3 shows the relationships between the condensation energies for the isolated compounds and the molecules in solution. Almost linear relationships are observed ($R^2 > 0.95$), demonstrating that solvent effects have mostly quantitative effects on these equilibria, but no qualitative effects.

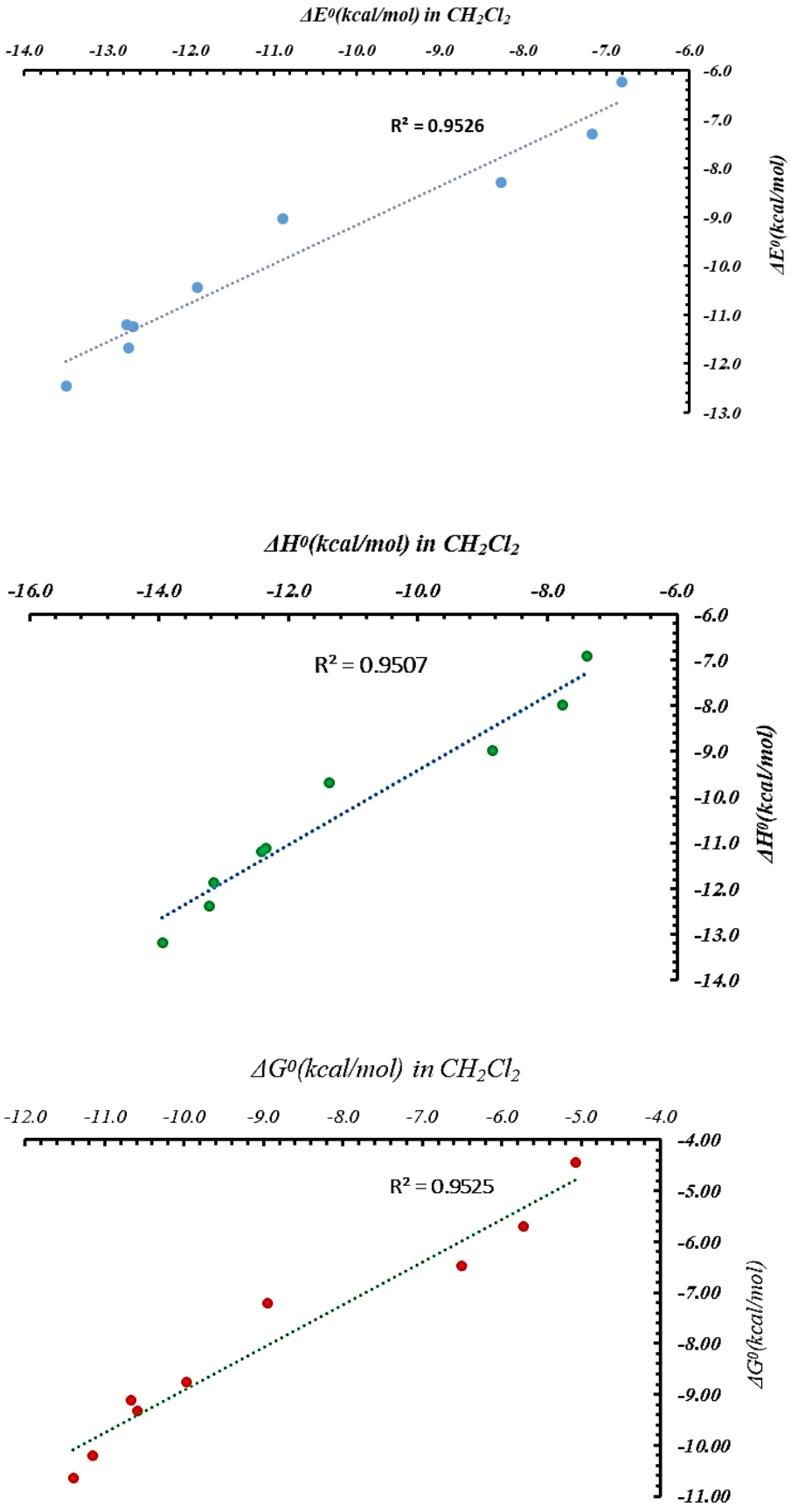

Fig. IV.3: Comparison between the thermodynamical values (ΔE as well as ΔH^0 and ΔG^0 at 298.15 K) of the reaction of condensation obtained in gas phase and in CH_2Cl_2 (IEF-PCM). All calculations were performed at the MP2/cc-pVTZ level of approximation.

IV.2.2. Other wave function methods

In this section, the ΔE^0 values were calculated at the HF, CID, CISD, CCD, CCSD, MP2, MP3, MP4SD, MP4SDQ levels of approximation (Fig. **IV.4**, Tables **IV.5** and **IV.6**). The CCSD method provides reference values. As expected, the CID and CISD values are far, which is attributed to the lack of size consistency of these truncated CI schemes. For the other methods, linear regressions between their values and the reference CCSD ones were performed (Fig. **IV.4** and Table **IV.7**). In all the cases, very good regression coefficients were obtained.

On the one hand, the HF method systematically overestimates the ΔE^0 values, by 6 to 7 kcal/mol in gas phase and even slightly more in CH_2Cl_2. On the other hand, the MP2 method systematically underestimates the ΔE^0 values, by 4-5 kcal/mol in both phases. Improved results are obtained at the MP4DQ and even more at the MP4SDQ and CCD levels of approximation. This is obvious on the Figures but also by considering the slope of the linear regression equation (closer and closer to 1.0) and the intercept at the origin, which gets negligibly small.

Table IV.5: Gas phase ΔE^0 values (kcal/mol) as calculated at different levels of approximation.

Compounds	HF	CID	CISD	MP2	MP4DQ	MP4SDQ	CCD	CCSD
1	-2.7	133.6	134.9	-13.5	-9.0	-8.4	-9.6	-9.3
2	-1.4	134.4	135.6	-12.7	-8.0	-7.3	-8.6	-8.2
3	0.1	135.8	137.1	-11.9	-7.1	-6.4	-7.7	-7.3
4	3.0	141.8	143.2	-8.3	-3.7	-3.0	-4.3	-3.9
5	-2.3	136.2	137.5	-12.7	-8.4	-7.6	-9.0	-8.6
6	-0.0	138.9	140.3	-10.9	-6.5	-5.6	-7.0	-6.7
7	5.3	142.5	143.9	-6.8	-2.4	-1.4	-2.7	-2.3
8	-3.3	135.2	136.6	-12.8	-8.8	-8.3	-9.3	-9.1
9	4.1	141.4	142.9	-7.2	-2.6	-1.9	-3.2	-2.8

Table IV.6 CH_2Cl_2 ΔE^0 values (kcal/mol) as calculated at different levels of approximation.

Compounds	HF	CID	CISD	MP2	MP4DQ	MP4SDQ	CCD	CCSD
1	-1.2	135.0	136.4	-12.5	-9.0	-7.4	-8.5	-8.5
2	0.8	136.3	137.6	-11.7	-7.7	-6.0	-7.3	-7.1
3	2.2	137.8	139.0	-10.4	-6.6	-4.9	-6.2	-6.0
4	3.4	142.0	143.5	-8.3	-4.7	-3.0	-4.3	-4.1
5	-0.1	138.3	139.7	-11.2	-7.9	-6.1	-8.4	-7.2
6	2.1	140.1	142.5	-9.0	-5.7	-4.0	-5.3	-5.1
7	6.3	143.2	144.7	-6.2	-2.7	-0.8	-2.2	-1.9
8	-1.6	137.0	138.4	-11.2	-8.3	-6.9	-7.8	-7.9
9	4.9	141.1	143.4	-7.3	-3.5	-1.9	-3.0	-3.1

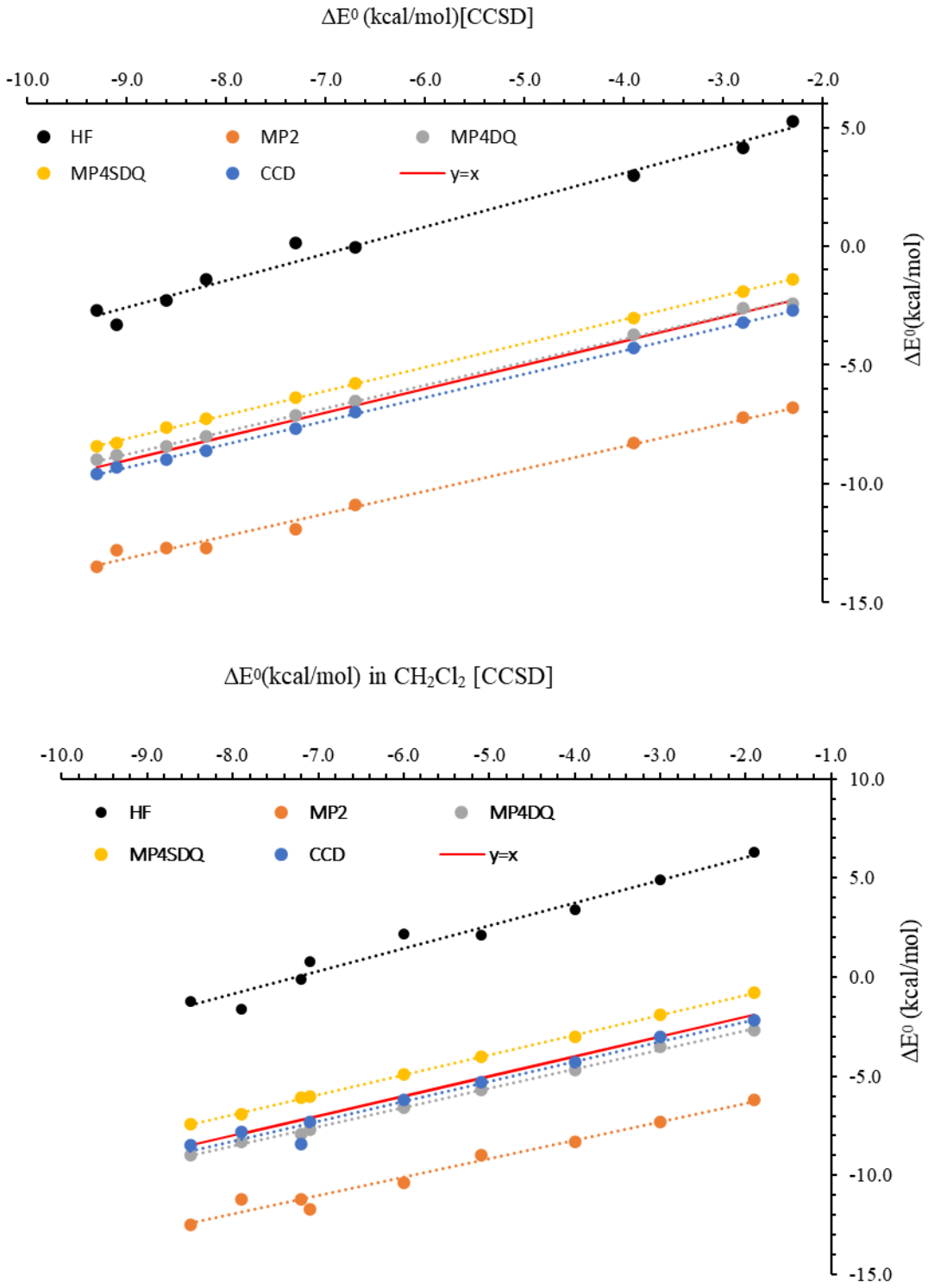

Fig. IV.4: Relationships between the ΔE^0 values evaluated at different levels of approximation and the reference CCSD ΔE^0 values for the reaction of condensation (a) in gas phase and (b) in CH_2Cl_2 (IEF-PCM). All values are given in kcal/mol.

Table. IV.7: Linear regressions related to **Fig. IV.3**.

Methods	Equation	R^2
	Isolated molecules	
HF	$\Delta E^0_{HF} = 1.1267\ \Delta E^0_{CCSD} + 7.5911$	0.9827
MP2	$\Delta E^0_{MP2} = 0.9477\ \Delta E^0_{CCSD} - 4.6272$	0.9919
MP4DQ	$\Delta E^0_{MP4DQ} = 0.9863\ \Delta E^0_{CCSD} - 0.4444$	0.9991
MP4SDQ	$\Delta E^0_{MP4SDQ} = 0.999\ \Delta E^0_{CCSD} + 0.9069$	0.997
CCD	$\Delta E^0_{CCD} = 0.9704\ \Delta E^0_{CCSD} - 0.002$	0.9995
	CH_2Cl_2	
HF	$\Delta E^0_{HF} = 1.1531\ \Delta E^0_{CCSD} + 8.3627$	0.9644
MP2	$\Delta E^0_{MP2} = 0.9307\ \Delta E^0_{CCSD} - 4.5198$	0.9744
MP4DQ	$\Delta E^0_{MP4DQ} = 0.9707\ \Delta E^0_{CCSD} - 0.7653$	0.9979
MP4SDQ	$\Delta E^0_{MP4SDQ} = 1.0015\ \Delta E^0_{CCSD} + 1.0563$	0.9996
CCD	$\Delta E^0_{CCD} = 1.0072\ \Delta E^0_{CCSD} - 0.2148$	0.9734

IV.3. Thermodynamics of the condensation reactions using DFT and different XC functionals

DFT was then applied, using a selection of XC functionals. In this case, full geometry optimizations were also carried out and the different-thermodynamic quantities were evaluated in gas phase and in CH_2Cl_2 (IEF-PCM). The list of functionals and some of their characteristics are given in Table II.1 (See Chapter II on Methodological and Computational Aspects). This selection was made to sample the different rungs of Jacob's ladder. The whole list of results is given in Appendix for the successive 9 anil derivatives. The following paragraphs tackle the performance of these DFT XC functionals with respect to wavefunction methods.

IV.3.1. ΔE^0 (DFT-XC) in comparison to ΔE^0 (CCSD) and ΔE^0 (MP2)

ΔE^0 is a first approximation to the thermodynamical state functions. It is the easiest to calculate since vibrational frequencies are not necessary for their evaluations. This explains why it was possible to perform CCSD calculations and to use these as reference. Nevertheless, since MP2 is the reference for the other thermodynamical quantities, the MP2 ΔE^0 values are also used for comparisons. The results are listed in Tables **IV.8** and **IV.9**. Then, Fig. **IV.5** highlights good linear relationships between the reference CCSD results and those obtained with any other level of approximation. For the sake of completeness, we remind that both in gas phase and in solvent, the MP2 method leads to too negative ΔE^0 values (by about 4-5 kcal/mol) in comparison to CCSD. This aspect should be taken into account when assessing the performance of DFT XC functionals to get temperature-dependent thermodynamical state functions. One XC functional, SVWN, the simplest XC employed here gives similar results to MP2. On the other hand, all the other XC functionals overestimate the energies of condensation. In some cases, these ΔE^0 values are even positive whereas all CCSD values are negative. So, these XC functionals do not predict a gain in energy when forming the *N*-salicylideneanilines, both in gas phase and in solution. This appears as a strong limitation of these functionals.

The regression equations are listed in Table VI.10. All regressions have good R^2 values, of 0.95 for SVWN and larger than 0.985 for all other functionals. Among all the DFT results, those obtained with the double hybrid B2PLYP XC functional are the closest to the CCSD values, with typical deviations of 1-2 kcal/mol, both in gas phase and in solution. Thus, the double-hybrid B2PLYP behaves quite differently from the MP2 method (their computational costs are similar). Then comes the ωB97X-D XC with deviations of 2-3 kcal/mol, again both in gas phase and in solution. Nevertheless, with respect to B2PLYP, it is computationally much advantageous because no MP2 correlation energy is calculated. Among these functionals the worst is M05. Then comes ωB97, probably because it is not well-balanced (it has no HF exchange at short-range).

Table. IV.8. ΔE^0 of the reaction of condensation to prepare the enol form as calculated by DFT-XC, MP2, and CCSD methods in gas phase. All values are given in (kcal/mol).

Method	1	2	3	4	5	6	7	8	9
CCSD	-9.3	-8.2	-7.3	-3.9	-8.6	-6.7	-2.3	-9.1	-2.8
MP2	-13.5	-12.7	-11.9	-8.3	-12.7	-10.9	-6.8	-12.8	-7.2
B2PLYP	-8.5	-7.6	-6.5	-3.0	-7.4	-5.8	-1.4	-8.1	-2.2
B3LYP	-6.1	-5.3	-4.0	-0.7	-4.9	-3.5	1.0	-5.8	0.0
BLYP	-5.4	-4.6	-3.6	-0.1	-4.2	-2.8	1.3	-5.0	0.4
M05	-3.8	-2.5	-1.6	1.6	-2.2	-1.1	3.4	-3.7	2.9
M06	-6.0	-5.0	-3.8	-0.4	-4.6	-3.2	1.3	-5.7	0.5
SVWN	-12.9	-12.5	-10.8	-7.1	-11.2	-9.7	-5.5	-12.1	-7.0
TPSS	-5.9	-5.3	-3.9	-0.6	-4.9	-3.2	1.0	-5.5	-0.2
ωB97	-5.3	-3.9	-2.9	0.3	-3.8	-2.4	2.2	-5.2	1.7
ωB97X	-5.8	-4.5	-3.6	-0.3	-4.4	-3.0	1.6	-5.7	1.0
ωB97X-D	-6.5	-5.9	-5.0	-1.7	-5.6	-4.3	0.1	-6.9	-0.4

Table. IV.9. ΔE^0 of the reaction of condensation to prepare the enol form as calculated by DFT-XC, MP2, and CCSD methods in CH_2Cl_2 (IEF-PCM). All values are given in (kcal/mol).

Method	1	2	3	4	5	6	7	8	9
CCSD	-8.5	-7.1	-6.0	-4.1	-7.2	-5.1	-1.9	-7.9	-3.1
MP2	-12.5	-11.7	-10.4	-8.3	-11.2	-9.0	-6.2	-11.2	-7.3
B2PLYP	-7.0	-6.0	-4.5	-2.6	-5.4	-3.4	-0.4	-6.2	-1.8
B3LYP	-4.5	-3.5	-1.9	0.0	-2.8	-0.8	2.2	-3.7	0.7
BLYP	-3.7	-2.9	-1.4	0.6	-2.0	-0.2	2.6	-2.8	1.1
M05	-2.8	-1.5	-0.1	1.7	-0.7	0.6	3.8	-2.8	2.8
M06	-4.4	-3.3	-1.7	0.2	-2.5	-0.7	2.4	-3.7	1.0
SVWN	-11.4	-11.0	-8.7	-6.5	-9.2	-6.8	-4.2	-9.8	-6.5
TPSS	-4.3	-3.6	-1.8	0.0	-2.7	-0.6	2.2	-3.5	0.5
ωB97	-3.9	-2.2	-1.0	0.7	-1.9	-0.2	3.1	-3.4	2.0
ωB97X	-4.4	-2.9	-1.6	0.2	-2.4	-0.7	2.6	-3.8	1.4
ωB97X-D	-6.0	-4.2	-2.9	-1.1	-3.5	-1.9	1.2	-4.9	0.1

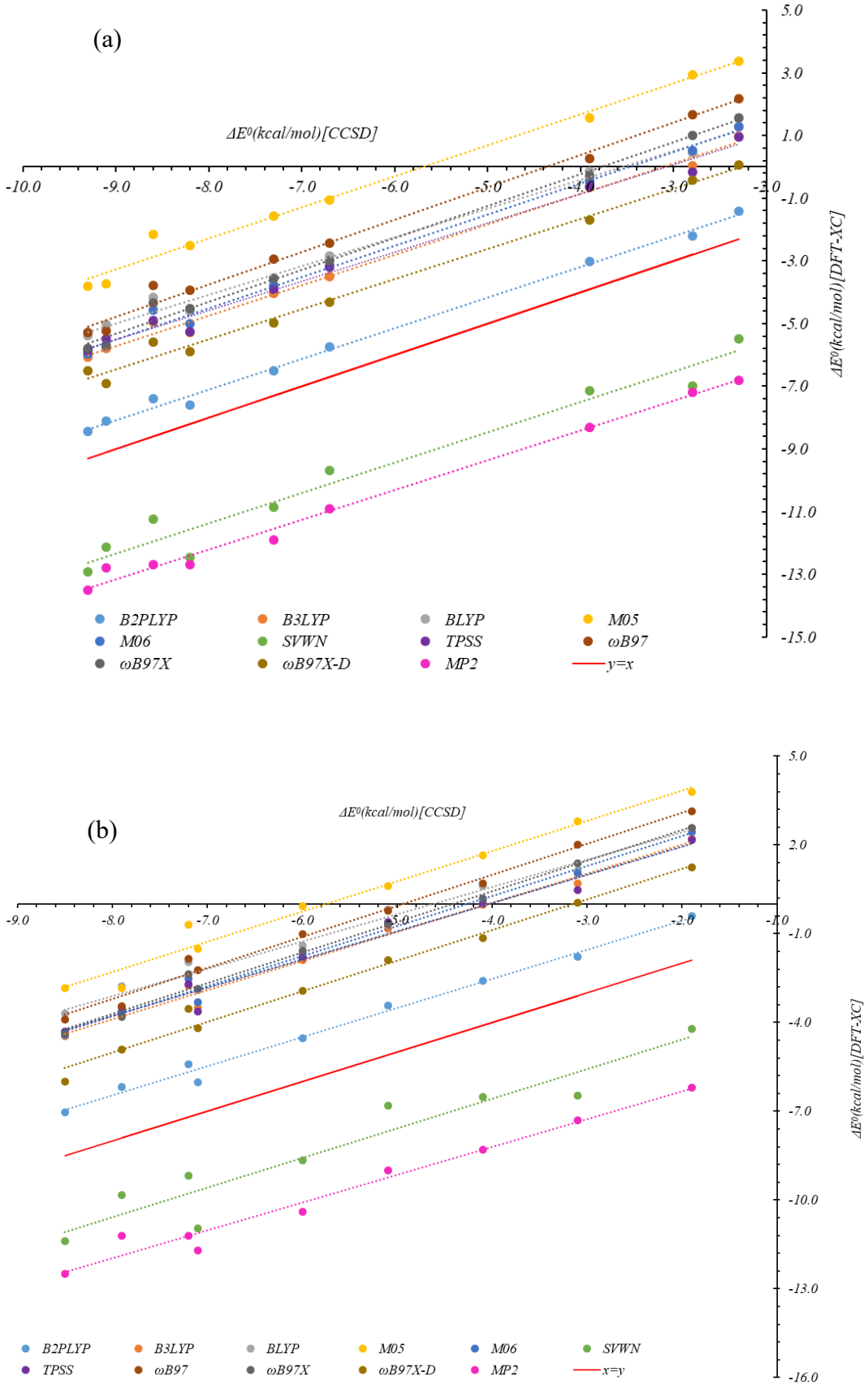

Fig.I V.5. Relationships between the ΔE^0 values (kcal/mol) evaluated at the DFT-XC, MP2, and the corresponding reference CCSD levels. (a) in gas phase and (b) in CH_2Cl_2 (IEF-PCM).

IV.3.2. ΔH^0 (DFT-XC) in comparison to ΔH^0 (MP2)

Keeping in mind that the MP2 ΔE^0 values are too negative, we now compare the enthalpies of reaction calculated with the different XC functionals with the MP2 ones, in gas phase and in solution (Fig. IV.6 and Table IV.10 and Table IV.11). The objective is to check whether the performance of the XC functionals is the same after including these thermal effects. As expected, there is a good consistency between these ΔH^0 results and the ΔE^0 values of the previous paragraph. So, the SVWN ΔH^0 values are close to the MP2 reference. It is noteworthy that the next XC functional is B2PLYP, in both phases, with differences of about 6 kcal/mol. Based on the results of paragraph IV.3.1, an alternative would have been to consider B2PLYP as a new reference but we have preferred continuing with a wavefunction-based reference method, namely MP2. The next XC functional in order of decreasing performances is ωB97X-D and the worst is again M05, followed by ωB97. Note that M06, which is similar in content to M05, provides improved results by about 2 kcal/mol. For all methods, good linear regressions with respect to the reference MP2 results were obtained. The regression equations are listed in Table VI.11 of the appendix.

Table IV.10. ΔH^0 (T = 298.15K) of the reaction of condensation to prepare the enol form as calculated by DFT-XC and MP2 methods in gas phase. All values are given in kcal/mol.

Method	1	2	3	4	5	6	7	8	9
MP2	-13.9	-13.2	-12.4	-8.9	-12.4	-11.4	-7.4	-13.2	-7.8
B2PLYP	-8.9	-8.1	-6.9	-3.6	-7.0	-6.2	-2.0	-8.5	-2.8
B3LYP	-6.5	-5.7	-4.5	-1.2	-4.6	-3.8	0.4	-6.1	-0.6
BLYP	-5.8	-5.1	-4.1	-0.8	-4.0	-3.3	0.6	-5.4	-0.3
M05	-4.1	-2.8	-1.9	1.2	-1.7	-1.3	3.0	-3.9	2.5
M06	-6.0	-5.1	-3.9	-0.7	-3.9	-3.3	1.1	-5.7	0.3
SVWN	-13.7	-13.5	-11.7	-8.2	-11.3	-10.4	-6.5	-12.8	-8.0
TPSS	-6.4	-5.9	-4.5	-1.4	-4.8	-3.8	0.2	-6.0	-1.0
ωB97	-5.5	-4.1	-3.3	-0.2	-3.3	-2.7	1.8	-5.5	1.2
ωB97X	-6.0	-4.7	-3.8	-0.6	-3.8	-3.2	1.2	-5.9	0.6
ωB97X-D	-7.2	-6.1	-5.2	-2.0	-5.1	-4.5	-0.2	-7.0	-0.7

Table IV.11. ΔH^0 (T = 298.15K) of the reaction of condensation to prepare the enol form as calculated by DFT-XC and MP2 methods in CH_2Cl_2. All values are given in kcal/mol.

Method	1	2	3	4	5	6	7	8	9
MP2	-13.2	-12.4	-11.2	-9.0	-11.1	-9.7	-6.9	-11.9	-8.0
B2PLYP	-7.7	-6.7	-5.3	-3.3	-5.3	-4.1	-1.1	-6.8	-2.6
B3LYP	-5.1	-4.2	-2.6	-0.7	-2.7	-1.5	1.5	-4.3	-0.1
BLYP	-4.5	-3.7	-2.2	-0.2	-2.1	-1.0	1.7	-3.5	0.2
M05	-3.3	-1.9	-0.6	1.2	-0.4	0.4	3.5	-2.7	2.4
M06	-4.7	-3.6	-2.0	-0.2	-2.1	-0.9	2.1	-3.9	0.7
SVWN	-12.4	-12.3	-9.8	-7.7	-9.7	-7.8	-5.5	-10.7	-8.0
TPSS	-5.1	-4.5	-2.7	-0.8	-2.9	-1.4	1.3	-4.1	-0.5
ωB97	-4.4	-2.7	-1.5	0.2	-1.6	-0.7	2.7	-3.9	1.5
ωB97X	-4.9	-3.4	-2.1	-0.3	-2.1	-1.2	2.1	-4.3	0.9
ωB97X-D	-7.2	-4.7	-3.4	-1.6	-3.3	-2.3	0.7	-5.3	-1.1

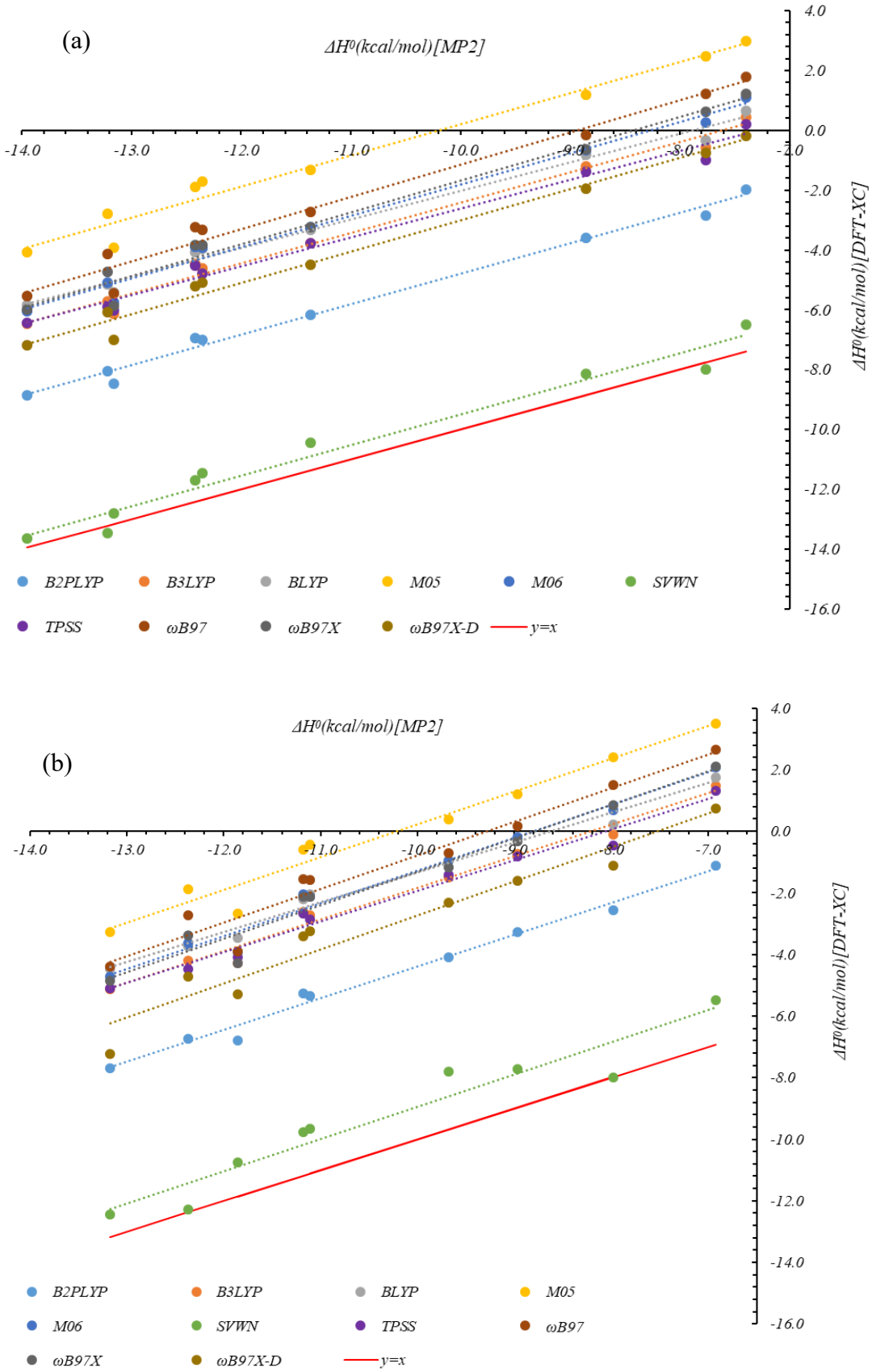

Fig. IV.6. Relationships between the ΔH^0 (T = 298.15K, kcal/mol) values evaluated at the DFT-XC and the corresponding reference MP2 values. (a) in gas phase and (b) in CH_2Cl_2 (IEF-PCM).

IV.3.3. ΔG^0 (DFT-XC) in comparison to ΔG^0 (MP2)

When discussing equilibrium constant, the key thermodynamic quantity is the Gibbs enthalpy. Following the same approach and levels of approximation as for ΔG^0 these results are given in Fig. IV.7 and Table IV.12 and Table IV.13. These results follow the same trends as those analyzed for the ΔH^0 values. The corresponding linear relationships are given in table VI.13 in the appendix. The similarity between ΔE^0, ΔH^0, and ΔG^0 comes from the fact that the electronic energy contribution is dominant. Therefore, it calls for a more precise investigation of the different vibrational and thermal contributions to ΔH^0 and ΔG^0.

Table 12. ΔG^0 (T = 298.15K) of the reaction of condensation to prepare the enol form as calculated by DFT-XC and MP2 methods in gas phase. All values are given in kcal/mol.

Method	1	2	3	4	5	6	7	8	9
MP2	-11.4	-11.2	-10.0	-6.5	-10.7	-9.0	-5.1	-10.6	-5.7
B2PLYP	-6.5	-6.3	-4.7	-1.4	-5.6	-4.0	0.2	-6.1	-1.1
B3LYP	-4.2	-3.8	-2.2	0.9	-3.1	-1.6	2.6	-3.8	1.4
BLYP	-3.7	-3.4	-2.0	1.1	-2.7	-1.3	2.6	-3.3	1.5
M05	-1.9	-1.0	0.2	3.2	-0.4	0.8	5.1	-1.7	4.4
M06	-3.9	-3.3	-1.9	1.3	-2.6	-1.3	3.3	-3.7	2.0
SVWN	-11.7	-11.3	-9.7	-5.9	-10.3	-8.0	-5.1	-10.6	-6.0
TPSS	-4.4	-4.1	-2.6	0.5	-3.5	-2.0	2.1	-4.0	0.8
ωB97	-3.0	-2.1	-0.9	2.1	-1.7	-0.3	4.1	-2.9	3.3
ωB97X	-3.5	-2.7	-1.6	1.6	-2.2	-0.9	3.6	-3.4	2.6
ωB97X-D	-4.9	-4.3	-2.9	0.4	-3.7	-2.1	2.2	-4.5	1.1

Table 13. ΔG^0 (T = 298.15K) of the reaction of condensation to prepare the enol form as calculated by DFT-XC and MP2 methods in CH_2Cl_2. All values are given in kcal/mol.

Method	1	2	3	4	5	6	7	8	9
MP2	-10.6	-10.2	-8.8	-6.5	-9.1	-7.2	-4.5	-9.3	-5.7
B2PLYP	-5.5	-5.2	-3.1	-1.1	-3.9	-1.9	1.1	-4.6	-1.0
B3LYP	-2.9	-2.6	-0.4	1.4	-1.4	0.7	3.8	-2.1	1.5
BLYP	-2.4	-2.0	-0.2	1.8	-0.6	1.1	3.9	-1.4	1.9
M05	-1.1	0.1	1.6	3.4	1.2	2.7	5.8	-0.4	4.6
M06	-2.7	-1.9	-0.1	1.9	-0.8	1.1	4.6	-2.0	2.5
SVWN	-10.2	-10.1	-7.1	-5.2	-8.0	-5.1	-3.1	-8.3	-5.3
TPSS	-2.9	-2.7	-0.5	1.4	-1.4	0.8	3.6	-1.9	1.5
ωB97	-2.1	-0.8	0.7	2.4	0.2	1.6	5.2	-1.5	3.7
ωB97X	-2.8	-1.7	-0.2	1.7	-0.7	0.8	4.5	-2.2	2.5
ωB97X-D	-4.8	-3.0	-1.1	0.6	-1.6	0.1	3.2	-2.9	2.1

(a)

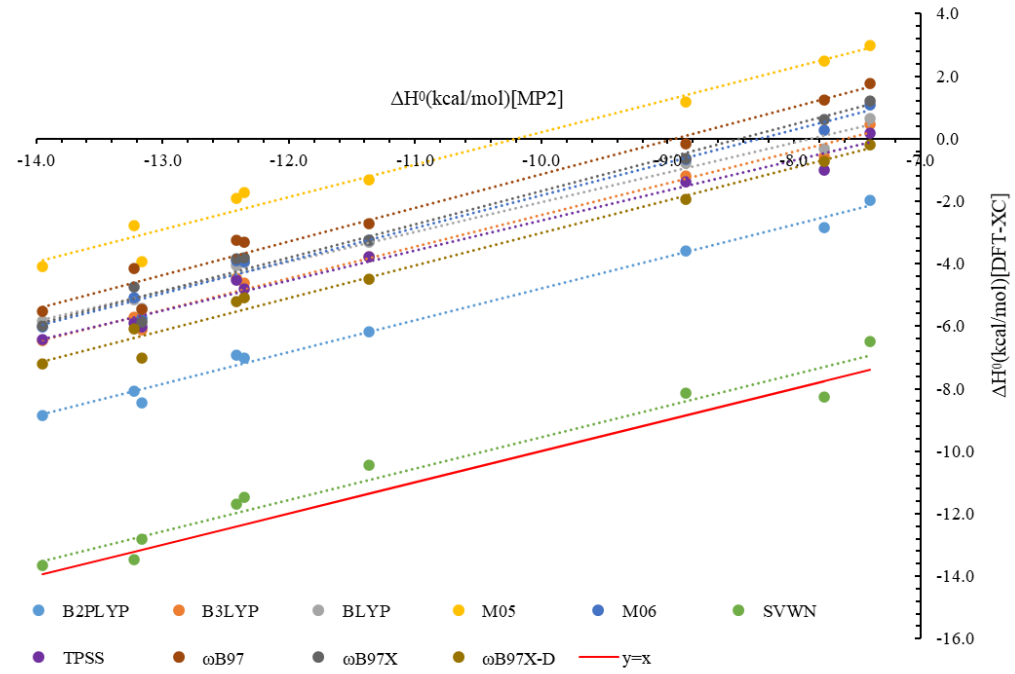

(b)

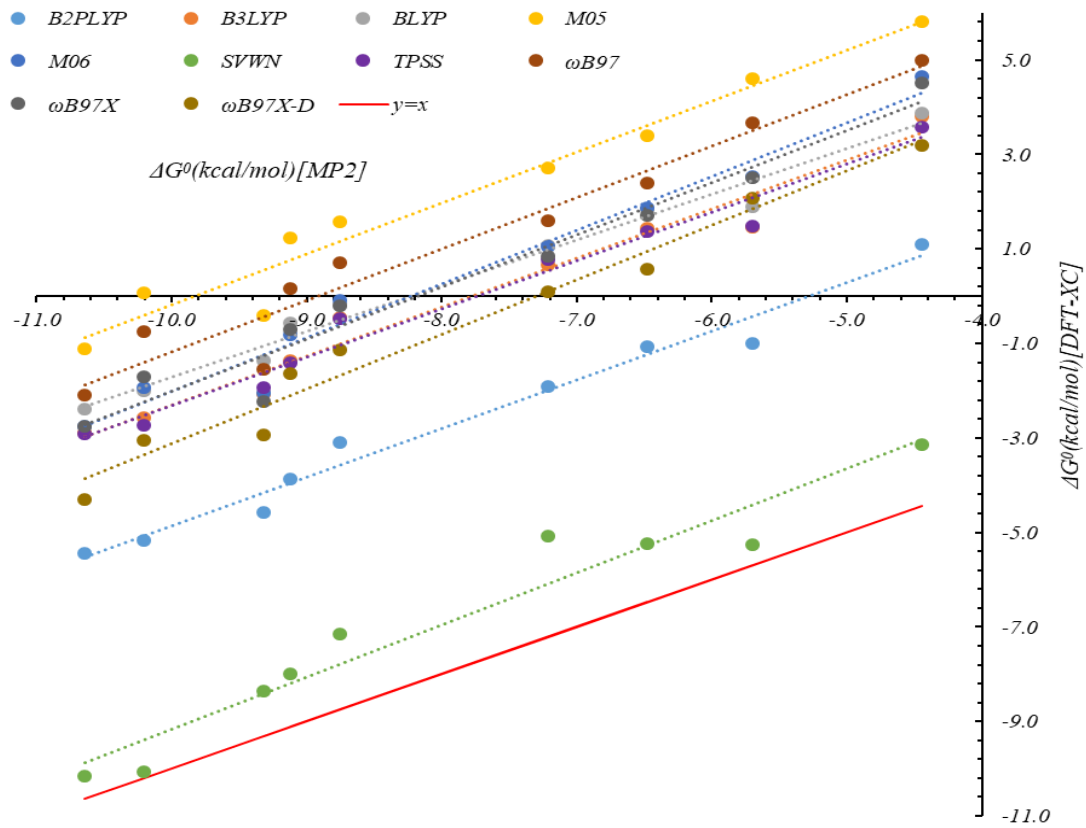

Fig. IV.7. Relationships between the ΔG^0 (T = 298.15K, kcal/mol) values evaluated at the DFT-XC and the corresponding reference MP2 values. (a) in gas phase and (b) in CH_2Cl_2 (IEF-PCM).

IV. 3.4. ΔS^0 (DFT-XC) in comparison to ΔS^0 (MP2)

In order to get more insight into the different contributions to ΔG^0 we continue here by analyzing the entropic contributions to the reactions of condensation to prepare the N-salicylideneaniline species in their enol forms. The results of our calculations are presented in Fig. **IV.8**, Table **IV.14** and **IV.15** while the regression equations and coefficients are listed in table VI-12 in appendix. It is noticeable that there is no good relationship between the MP2 reference and the SVWN values, either in gas phase or in solution. The same occurs for M05 and M06 when accounting for solvent effects. This is attributed to the poorest performance of these XC functionals. Concerning B2PLYP and ωB97X-D, the correlation coefficients are satisfactory. Still, the slopes of the equations can be far from 1.0, especially in solution. Although, for time reasons, it was not possible to assess these effects, it might have been interesting to see whether there is a correlation between these slopes (how much they differ from 1.0) and the vibrational frequencies.

Table.14. ΔS^0 (T = 298.15K) of the reaction of condensation to prepare the enol form as calculated by DFT-XC and MP2 methods in gas phase. All values are given in cal/mol K.

Method	1	2	3	4	5	6	7	8	9
MP2	-8.6	-6.9	-8.2	-7.9	-5.7	-8.1	-7.8	-8.6	-6.8
B2PLYP	-7.8	-6.0	-7.6	-7.3	-4.6	-7.5	-7.3	-7.9	-5.7
B3LYP	-7.7	-6.4	-7.6	-7.1	-5.1	-7.3	-7.3	-7.7	-6.5
BLYP	-7.1	-5.9	-6.9	-6.5	-4.3	-6.7	-6.7	-7.1	-6.0
M05	-7.3	-6.1	-7.2	-6.8	-4.6	-7.2	-7.1	-7.5	-6.6
M06	-7.2	-5.9	-6.6	-6.6	-4.6	-6.6	-7.3	-6.8	-5.9
SVWN	-6.7	-7.2	-6.7	-7.6	-3.8	-8.3	-7.7	-7.5	-7.6
TPSS	-6.9	-6.0	-6.5	-6.2	-4.5	-6.1	-6.4	-6.8	-6.0
ωB97	-8.3	-6.9	-7.9	-7.4	-5.3	-8.0	-7.7	-8.4	-7.0
ωB97X	-8.2	-6.7	-7.6	-7.5	-5.4	-7.7	-7.9	-8.1	-6.6
ωB97X-D	-7.9	-5.9	-7.7	-7.9	-4.7	-7.9	-7.9	-8.3	-6.3

Table.15. ΔS^0 of condensation for the enol form as calculated by DFT-XC and MP2 methods in CH_2Cl_2. All values are given in cal/mol K.

Method	1	2	3	4	5	6	7	8	9
MP2	-8.5	-7.2	-8.2	-8.4	-6.7	-8.3	-8.3	-8.5	-7.6
B2PLYP	-7.5	-5.3	-7.2	-7.4	-4.9	-7.3	-7.5	-7.4	-5.2
B3LYP	-7.5	-5.5	-7.3	-7.3	-4.6	-7.3	-7.8	-7.5	-5.2
BLYP	-7.0	-5.8	-6.8	-6.9	-5.0	-6.8	-7.2	-7.1	-5.6
M05	-7.3	-6.5	-7.2	-7.4	-5.5	-7.8	-8.9	-7.6	-7.3
M06	-6.6	-5.7	-6.5	-6.8	-4.4	-6.7	-8.6	-6.4	-6.2
SVWN	-7.7	-7.5	-8.8	-8.3	-5.6	-9.1	-7.8	-8.1	-9.2
TPSS	-7.3	-5.8	-7.3	-7.3	-4.8	-7.3	-7.6	-7.3	-6.5
ωB97	-7.7	-6.6	-6.7	-7.5	-5.8	-7.7	-8.7	-7.9	-7.2
ωB97X	-7.0	-5.6	-6.7	-6.8	-4.8	-6.8	-8.0	-6.9	-5.6
ωB97X-D	-8.0	-5.7	-7.6	-7.3	-5.5	-8.1	-8.2	-8.0	-7.6

(a)

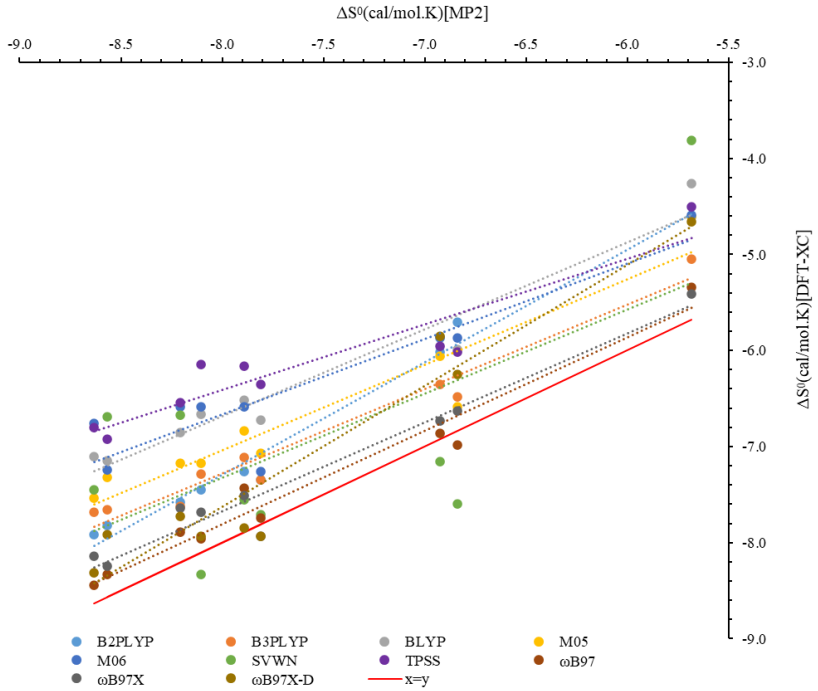

(b)

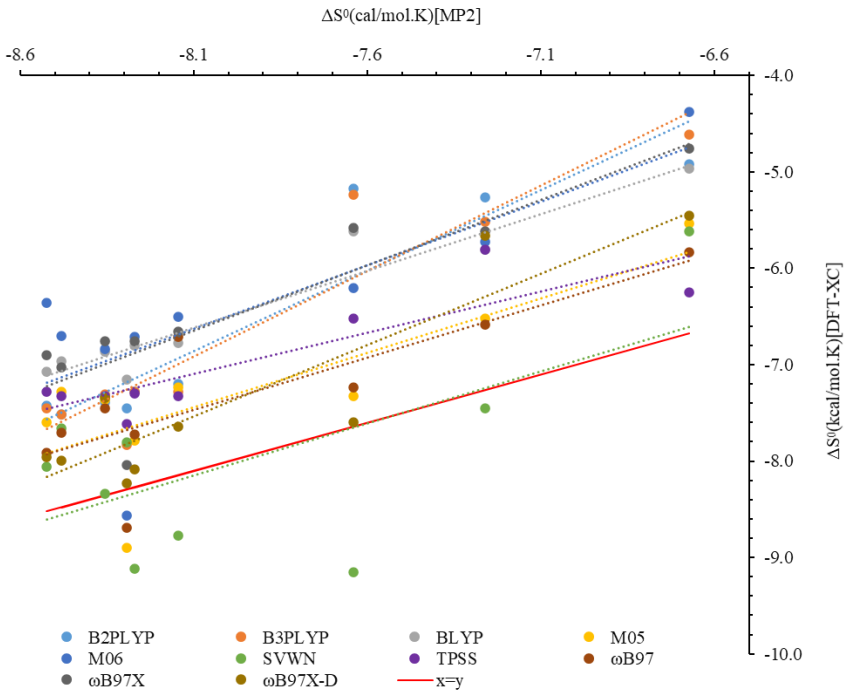

Fig.IV.8. Relationships between the ΔS^0 (T = 298.15K, cal/mol K) values evaluated at the DFT-XC and the corresponding reference MP2 values. (a) in gas phase and (b) in CH_2Cl_2 (IEF-PCM).

IV. 3.5. [$\Delta H^0 - \Delta E^0$] (DFT-XC) in comparison to [$\Delta H^0 - \Delta E^0$] (MP2)

In this paragraph, the vibrational and thermal corrections to the enthalpy have been calculated by DFT-XC and compared to the reference MP2 results (Fig. **IV.9** and Tables **IV.16** and **17**). There are good linear regressions between the DFT values and the reference MP2. Still, we do not stress on the regression equations because – even after double-check – the [$\Delta H^0 - \Delta E^0$] quantities for compound **5** are much different: they are positive whereas all the other ones are negative. For these corrections, the best agreement with MP2 is observed with B2PLYP as well as BLYP (gas phase) and B3LYP. When using SVWN (and, to a lower extent, TPSS), the amplitude of these [$\Delta H^0 - \Delta E^0$] corrections is overestimated. The opposite is observed for M06, M05, and also ωB97X-D. At this stage, there is no obvious correlation between these performances and the content of the XC functionals.

Table.16. [$\Delta H^0 - \Delta E^0$] (T = 298.15 K) values for the reactions of condensation to prepare the enol form of the N-salicylideneanilines as calculated at the DFT-XC and MP2 levels of approximation in gas phase. All values are given in (kcal/mol).

Methods	1	2	3	4	5	6	7	8	9
MP2	-0.5	-0.5	-0.5	-0.6	0.3	-0.5	-0.6	-0.4	-0.6
B2PLYP	-0.4	-0.5	-0.5	-0.6	0.4	-0.4	-0.6	-0.4	-0.6
B3LYP	-0.4	-0.4	-0.4	-0.5	0.3	-0.3	-0.5	-0.3	-0.6
BLYP	-0.5	-0.5	-0.5	-0.7	0.2	-0.5	-0.7	-0.4	-0.8
M05	-0.3	-0.3	-0.3	-0.4	0.4	-0.2	-0.4	-0.2	-0.5
M06	-0.1	-0.1	-0.1	-0.2	0.6	-0.1	-0.2	0.0	-0.3
SVWN	-0.7	-0.9	-0.9	-1.0	-0.1	-0.8	-1.0	-0.7	-1.1
TPSS	-0.6	-0.6	-0.6	-0.8	0.1	-0.6	-0.8	-0.5	-0.8
ωB97	-0.3	-0.2	-0.3	-0.4	0.5	-0.3	-0.4	-0.2	-0.4
ωB97X	-0.2	-0.2	-0.3	-0.4	0.5	-0.3	-0.3	-0.2	-0.4
ωB97X-D	-0.1	-0.2	-0.2	-0.3	0.5	-0.2	-0.3	-0.1	-0.3

Table.17. [$\Delta H^0 - \Delta E^0$] (T = 298.15 K) values for the reactions of condensation to prepare the enol form of the N-salicylideneanilines as calculated at the DFT-XC and MP2 levels of approximation in CH_2Cl_2. All values are given in (kcal/mol).

Methods	1	2	3	4	5	6	7	8	9
MP2	-0.7	-0.7	-0.7	-0.7	0.1	-0.7	-0.7	-0.7	-0.7
B2PLYP	-0.7	-0.7	-0.7	-0.7	0.1	-0.6	-0.7	-0.6	-0.8
B3LYP	-0.7	-0.7	-0.7	-0.7	0.0	-0.7	-0.7	-0.6	-0.7
BLYP	-0.8	-0.8	-0.8	-0.8	-0.1	-0.8	-0.8	-0.7	-0.8
M05	-0.4	-0.5	-0.5	-0.4	0.3	-0.4	-0.4	-0.4	-0.4
M06	-0.3	-0.3	-0.3	-0.3	0.4	-0.3	-0.3	-0.3	-0.4
SVWN	-1.0	-1.1	-1.1	-1.0	-0.5	-1.0	-1.1	-1.0	-1.0
TPSS	-0.8	-0.8	-0.9	-0.8	-0.1	-0.8	-0.9	-0.7	-0.8
ωB97	-0.5	-0.5	-0.5	-0.4	0.3	-0.5	-0.5	-0.5	-0.5
ωB97X	-0.5	-0.5	-0.5	-0.5	0.2	-0.5	-0.5	-0.5	-0.5
ωB97X-D	-0.5	-0.5	-0.5	-0.5	0.3	-0.4	-0.5	-0.4	-0.4

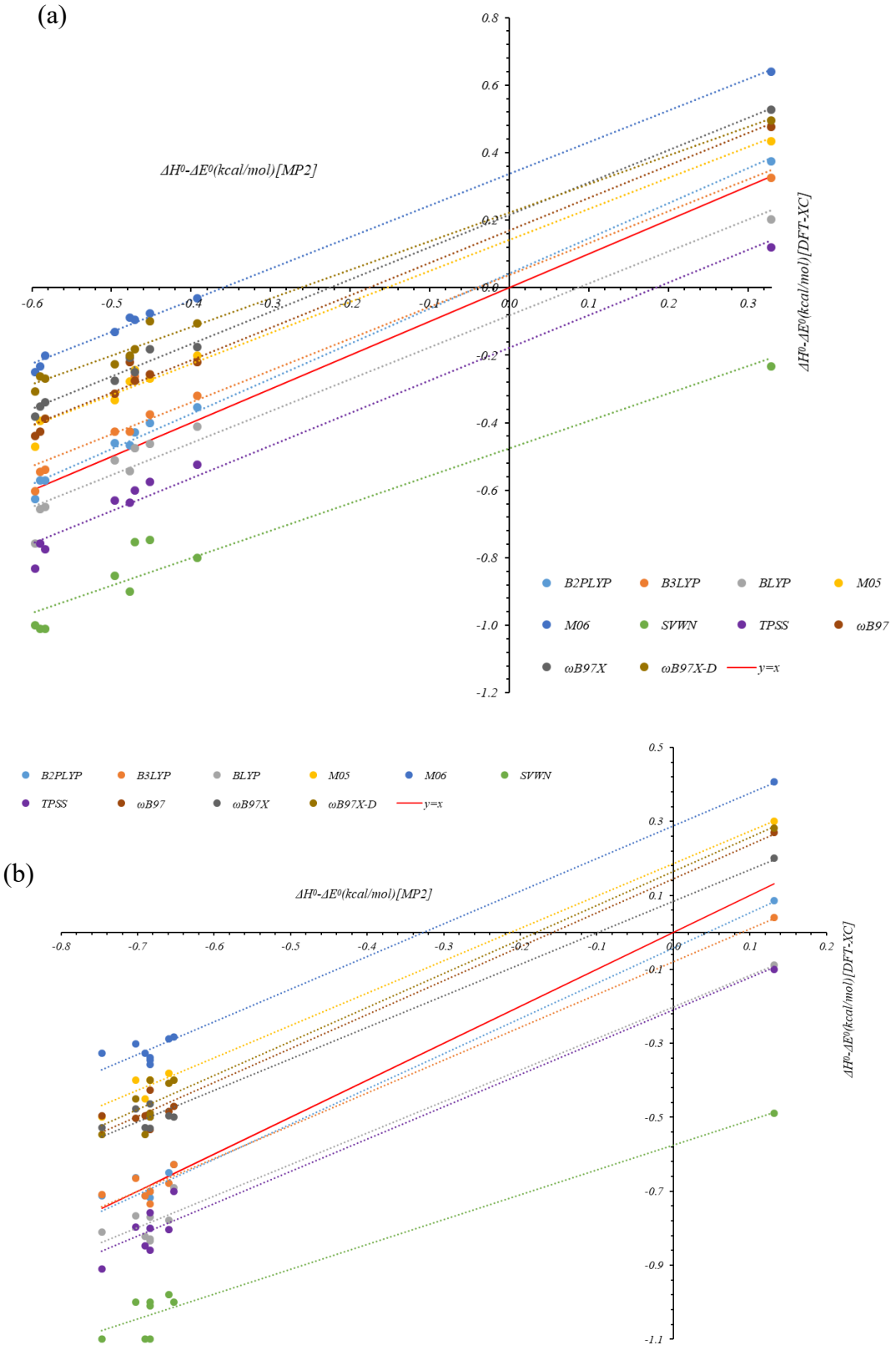

Fig.IV.9. Relationships between the [$\Delta H^0 - \Delta E^0$] (T = 298.15K, kcal/mol) values evaluated at the DFT-XC and the corresponding reference MP2 values. (a) in gas phase and (b) in CH_2Cl_2 (IEF-PCM).

IV. 3.6. $[\Delta G^0 - \Delta E^0]$ (DFT-XC) in comparison to $[\Delta G^0 - \Delta E^0]$ (MP2)

Finally, in this section, the vibrational and thermal corrections to the Gibbs enthalpy have been calculated by DFT-XC and compared to the reference MP2 results in Fig.IV.10 and Tables IV.18 and IV.19. Some correlation exists between the DFT-XC methods and the reference MP2 but not simple to analyze since the values span a narrow range of about 1 kcal/mol.

Table .18 $[\Delta G^0 - \Delta E^0]$ (T = 298.15 K) values for the reactions of condensation to prepare the enol form of the N-salicylideneanilines as calculated at the DFT-XC and MP2 levels of approximation in gas phase. All values are given in (kcal/mol).

Methods	1	2	3	4	5	6	7	8	9
MP2	2.1	1.6	2.0	1.8	2.0	1.9	1.7	2.1	1.4
B2PLYP	1.9	1.3	1.8	1.6	1.8	1.8	1.6	2.1	1.1
B3LYP	1.9	1.5	1.4	1.5	1.4	1.6	1.7	1.6	0.8
BLYP	1.7	1.2	1.2	1.2	1.4	1.3	1.4	1.4	0.8
M05	1.9	1.5	1.6	1.7	1.9	1.8	1.7	1.9	1.8
M06	2.1	1.7	1.6	1.7	1.7	2.2	2.0	1.6	1.5
SVWN	1.2	1.1	1.3	1.3	1.2	1.1	1.0	1.5	1.2
TPSS	1.5	1.1	1.3	1.3	1.3	1.4	1.1	1.6	1.0
ωB97	2.2	1.8	1.7	1.7	2.0	2.1	1.9	1.9	1.7
ωB97X	2.3	1.8	1.4	1.5	1.7	1.9	2.0	1.6	1.1
ωB97X-D	2.2	1.5	1.9	1.7	1.9	1.8	1.8	1.8	1.8

Table .19. $[\Delta G^0 - \Delta E^0]$ (T = 298.15 K) values for the reactions of condensation to prepare the enol form of the N-salicylideneanilines as calculated at the DFT-XC and MP2 levels of approximation in CH_2Cl_2. All values are given in (kcal/mol).

Methods	1	2	3	4	5	6	7	8	9
MP2	1.8	1.5	1.7	1.8	2.1	1.8	1.8	1.9	1.6
B2PLYP	1.6	0.9	1.4	1.5	1.6	1.5	1.5	1.6	0.8
B3LYP	1.6	0.9	1.4	1.5	1.4	1.5	1.6	1.6	0.8
BLYP	1.3	0.9	1.2	1.2	1.4	1.2	1.3	1.4	0.9
M05	1.7	1.5	1.6	1.7	1.9	1.9	1.8	1.9	1.1
M06	1.7	1.4	1.6	1.7	1.7	1.7	1.8	1.6	1.5
SVWN	1.2	0.9	1.5	1.3	1.2	1.7	1.1	1.5	1.2
TPSS	1.4	0.9	1.3	1.3	1.3	1.4	1.4	1.6	1.0
ωB97	1.8	1.5	1.7	1.7	2.0	1.8	1.9	1.9	1.6
ωB97X	1.6	1.1	1.4	1.5	1.7	1.5	1.9	1.6	1.1
ωB97X-D	1.9	1.1	1.8	1.7	1.8	1.8	1.8	1.8	1.8

(a)

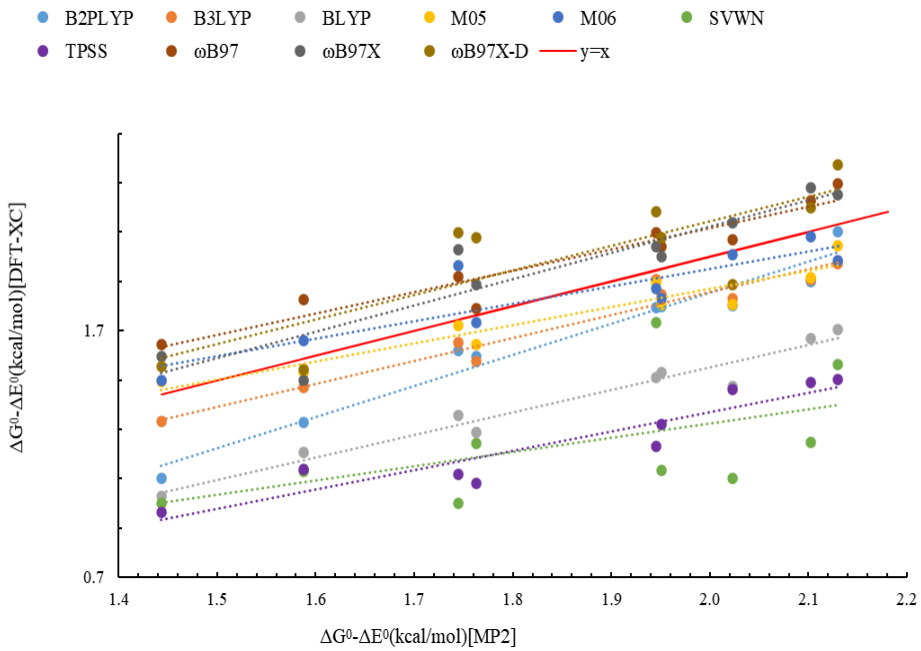

(b)

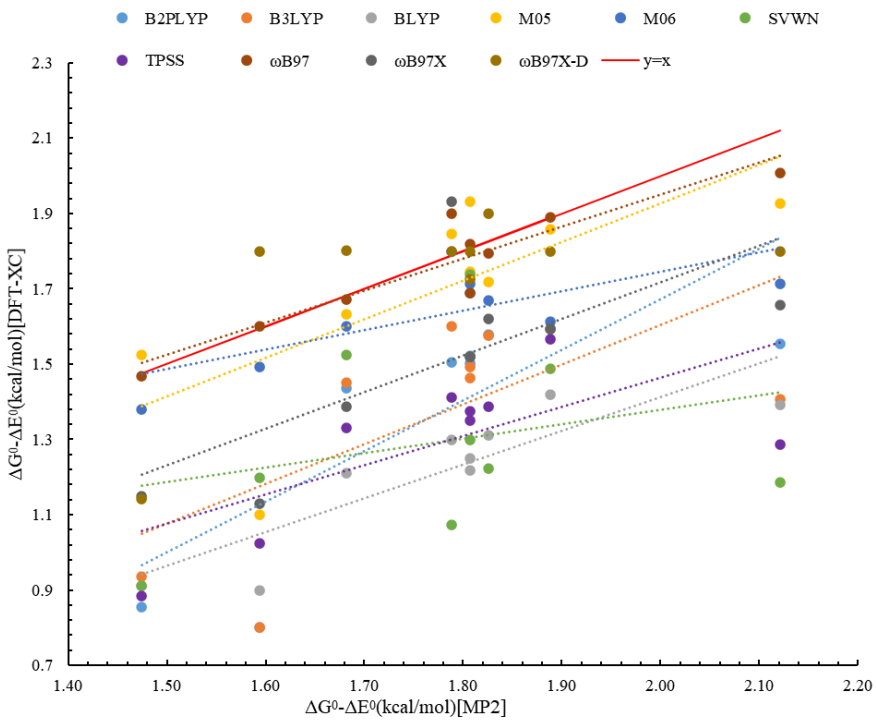

Fig.IV.10. Relationships between the [ΔG^0 - ΔE^0] (T = 298.15K, kcal/mol) values evaluated at the DFT-XC and the corresponding reference MP2 values. (a) in gas phase and (b) in CH_2Cl_2 (IEF-PCM).

V. FURTHER DISCUSSIONS, CONCLUSIONS AND OUTLOOK

In my Master Thesis, by using a broad range of quantum chemistry methods, I have investigated the reaction of condensation leading to the synthesis of N-salicylideneaniline derivatives.

First, reference ΔE^0 values have been evaluated at the CCSD level of approximation for the formation of the enol forms. All ΔE^0 values are negative, showing the process is favorable (without including at this stage the vibrational and thermal corrections). These reference CCSD values enable to calibrate other wavefunction methods, in particular the MP2 scheme, which was further used to evaluate the ΔE^0, ΔH^0, and ΔG^0 of reaction. In general, the MP2 scheme leads to ΔE^0 values 4-5 kcal/mol lower than the CCSD method. Similar results have been obtained for isolated molecules (gas phase) and in CH_2Cl_2, as described within the PCM scheme.

Then, DFT has been employed with a broad range of XC functionals, covering the different rungs of Jacob's ladder. The double hybrid B2PLYP XC functional gives ΔE^0 results that are the closest to the CCSD values, with typical deviations of 1-2 kcal/mol, both in gas phase and in solution. Then comes the ωB97X-D XC functional, which is computationally more advantageous than MP2 and B2PLYP. Still, even for the worst-performing XC functionals, good linear relationships were obtained with respect to the CCSD results (R^2 generally larger than 0.95). Similar relationships between MP2 and the different XC functionals have been observed for the ΔH^0 and ΔG^0 of reaction, demonstrating the dominant role of the electronic contributions to the "energies" of condensation. These results were an incentive to investigate in more details the entropic as well as thermal corrections. To a given extent, there are still correlations between the different levels of approximation but the R^2 values are smaller.

At the MP2 level, a more detailed investigation of the "energies" of reaction (ΔE^0, ΔH^0, and ΔG^0) has been achieved. A good consistency between the results in gas phase and in CH_2Cl_2 has been observed. The most exothermic ($\Delta H^0 < 0$) and exergonic ($\Delta G^0 < 0$) condensations occur for the anils with a single N substitution (N in position 3, then 2, then 4). Then come the condensations with two nitrogen atoms, with at least one in position 3. Moreover, by considering both the enol and keto forms, an assessment of the relationships between the ΔE^0 values and the torsion angle of the substituted ring has been non-conclusive. On the other hand, a reduction of this torsion angle has been evidenced when going from the enol to the keto form. When employing the MP2 level, it appears that for all N-salicylideneaniline derivatives except compound **9** in gas phase (and also compound **8** in CH_2Cl_2) the enol form is more stable (on the basis of ΔE^0 values) than the keto one. Due to time reasons, it was not possible to further characterize the enol-keto equilibrium, in particular by performing CCSD or B2PLYP calculations but this would be worth pursuing.

Besides the last issue, in order to extent our knowledge on these fascinating compounds and the deduction of structure-property relationships, future works can also encompass the simulation of the UV/vis absorption spectra. Moreover, from a quantum chemistry perspective, additional calculations could be performed to see whether some systematic variations of the thermodynamical properties can be related to the percentage of Hartree-Fock exchange, for both global hybrid and range-separated hybrids exchange-correlation functionals.

VI. APPENDIX

Table. **VI.1**. Thermodynamic values (kcal/mol) of the condensation reactions to form the enol tautomer **1** in gas phase and in CH_2Cl_2 (IEF-PCM) as calculated at the DFT level with different XC and the cc-pVTZ basis set.

Functional	ΔE^0(kcal/mol)		ΔU^0(kcal/mol)		ΔH^0(kcal/mol)		ΔG^0(kcal/mol)	
	Gas	solvent	Gas	solvent	Gas	solvent	Gas	solvent
B2PLYP	-8.5	-7.0	-8.9	-7.7	-8.9	-7.7	-6.5	-5.5
B3LYP	-6.1	-4.5	-6.5	-5.1	-6.5	-5.1	-4.2	-2.9
BLYP	-5.4	-3.7	-5.9	-4.5	-5.8	-4.5	-3.7	-2.4
M05	-3.8	-2.8	-4.1	-3.3	-4.1	-3.3	-1.9	-1.1
M06	-6.0	-4.4	-6.0	-4.7	-6.0	-4.7	-3.9	-2.7
SVWN	-12.9	-11.4	-13.7	-12.4	-13.7	-12.4	-11.7	-10.2
TPSS	-5.9	-4.3	-6.4	-5.1	-6.4	-5.1	-4.4	-2.9
ωB97	-5.3	-3.9	-5.5	-4.4	-5.5	-4.4	-3.0	-2.1
ωB97X	-5.8	-4.4	-6.0	-4.9	-6.0	-4.9	-3.5	-2.8
ωB97X-D	-6.5	-6.0	-7.2	-7.2	-7.2	-7.2	-4.9	-4.8

Table. **VI.2**. Thermodynamic values (kcal/mol) of the condensation reactions to form the enol tautomer **2** in gas phase and in CH_2Cl_2 (IEF-PCM) as calculated at the DFT level with different XC and the cc-pVTZ basis set.

Functional	ΔE^0(kcal/mol)		ΔU^0(kcal/mol)		ΔH^0(kcal/mol)		ΔG^0(kcal/mol)	
	Gas	solvent	Gas	solvent	Gas	solvent	Gas	solvent
B2PLYP	-7.6	-6.0	-8.1	-6.7	-8.1	-6.7	-6.3	-5.2
B3LYP	-5.3	-3.5	-5.7	-4.2	-5.7	-4.2	-3.8	-2.6
BLYP	-4.6	-2.9	-5.2	-3.7	-5.1	-3.7	-3.4	-2.0
M05	-2.5	-1.5	-2.8	-1.9	-2.8	-1.9	-1.0	0.1
M06	-5	-3.3	-5.1	-3.6	-5.1	-3.6	-3.3	-1.9
SVWN	-12.5	-11.0	-13.5	-12.3	-13.5	-12.3	-11.3	-10.1
TPSS	-5.3	-3.6	-5.9	-5.1	-5.9	-4.5	-4.1	-2.7
ωB97	-3.9	-2.2	-4.1	-2.7	-4.1	-2.7	-2.1	-0.8
ωB97X	-4.5	-2.9	-4.7	-3.4	-4.7	-3.4	-2.7	-1.7
ωB97X-D	-5.9	-4.2	-6.1	-4.7	-6.1	-4.7	-4.3	-3.0

Table. **VI.3**. Thermodynamic values (kcal/mol) of the condensation reactions to form the enol tautomer **3** in gas phase and in CH_2Cl_2 (IEF-PCM) as calculated at the DFT level with different XC and the cc-pVTZ basis set.

Functional	ΔE^0(kcal/mol)		ΔU^0(kcal/mol)		ΔH^0(kcal/mol)		ΔG^0(kcal/mol)	
	Gas	solvent	Gas	solvent	Gas	solvent	Gas	solvent
B2PLYP	-6.5	-4.5	-7.0	-5.3	-6.9	-5.3	-4.7	-3.1
B3LYP	-4	-1.9	-4.5	-2.6	-4.5	-2.6	-2.2	-0.4
BLYP	-3.6	-1.4	-4.0	-2.2	-4.1	-2.2	-2.0	-0.2
M05	-1.6	-0.1	-1.9	-0.6	-1.9	-0.6	0.2	1.6
M06	-3.8	-1.7	-3.9	-2.0	-3.9	-2.0	-1.9	-0.1
SVWN	-10.8	-8.7	-11.7	-9.8	-11.7	-9.8	-9.7	-7.1
TPSS	-3.9	-1.8	-4.5	-2.7	-4.5	-2.7	-2.6	-0.5
ωB97	-2.9	-1.0	-3.2	-14.7	-3.3	-1.5	-0.9	0.7
ωB97X	-3.6	-1.6	-3.8	-2.1	-3.8	-2.1	-1.6	-0.2
ωB97X-D	-5	-2.9	-5.2	-3.4	-5.2	-3.4	-2.9	-1.1

Table. **VI.4**. Thermodynamic values (kcal/mol) of the condensation reactions to form the enol tautomer **4** in gas phase and in CH_2Cl_2 (IEF-PCM) as calculated at the DFT level with different XC and the cc-pVTZ basis set.

Functional	**ΔE^0(kcal/mol)**		**ΔU^0(kcal/mol)**		**ΔH^0(kcal/mol)**		**ΔG^0(kcal/mol)**	
	Gas	solvent	Gas	solvent	Gas	solvent	Gas	solvent
B2PLYP	-2.6	0.8	-3.6	-3.3	-3.6	-3.3	-1.4	-1.1
B3LYP	0.0	-0.0	-1.2	-0.7	-1.2	-0.7	0.9	1.4
BLYP	0.6	0.6	-0.8	-0.2	-0.8	-0.2	1.1	1.8
M05	1.7	1.1	1.2	1.2	1.2	1.2	3.2	3.4
M06	0.2	0.2	-0.1	-0.2	-0.7	-0.2	1.3	1.9
SVWN	-6.5	-6.5	-8.2	-7.7	-8.2	-7.7	-5.9	-5.2
TPSS	0.0	0.0	-1.4	-0.8	-1.4	-0.8	0.5	1.4
ωB97	0.7	0.7	-0.2	0.2	-0.2	0.2	2.1	2.4
ωB97X	0.2	0.2	-0.6	-0.3	-0.6	-0.3	1.6	1.7
ωB97X-D	-1.1	-1.2	-1.6	-1.6	-2.0	-1.6	0.4	0.6

Table. **VI.5**. Thermodynamic values (kcal/mol) of the condensation reactions to form the enol tautomer **5** in gas phase and in CH_2Cl_2 (IEF-PCM) as calculated at the DFT level with different XC and the cc-pVTZ basis set.

Functional	**ΔE^0(kcal/mol)**		**ΔU^0(kcal/mol)**		**ΔH^0(kcal/mol)**		**ΔG^0(kcal/mol)**	
	Gas	solvent	Gas	solvent	Gas	solvent	Gas	solvent
B2PLYP	-7.4	-5.4	-7.1	-5.3	-7.0	-5.3	-5.6	-3.9
B3LYP	-4.9	-2.8	-4.6	-2.7	-4.6	-2.7	-3.1	-1.4
BLYP	-4.2	-2.0	-4.0	-2.0	-4.0	-2.1	-2.7	-0.6
M05	-2.2	-0.7	-1.7	-0.4	-1.7	-0.4	-0.4	1.2
M06	-4.6	-2.5	-3.9	-2.1	-3.9	-2.1	-2.6	-0.8
SVWN	-11.2	-9.2	-11.5	-9.7	-11.3	-9.7	-10.3	-8.0
TPSS	-4.9	-2.7	-5.1	-6.4	-4.8	-2.9	-3.5	-1.4
ωB97	-3.8	-1.9	-3.3	-2.7	-3.3	-1.6	-1.7	0.2
ωB97X	-4.4	-2.4	-3.8	-2.0	-3.8	-2.1	-2.2	-0.7
ωB97X-D	-5.6	-3.5	-5.1	-0.4	-5.1	-3.3	-3.7	-1.6

Table. **VI.6**. Thermodynamic values (kcal/mol) of the condensation reactions to form the enol tautomer **6** in gas phase and in CH_2Cl_2 (IEF-PCM) as calculated at the DFT level with different XC and the cc-pVTZ basis set.

Functional	**ΔE^0(kcal/mol)**		**ΔU^0(kcal/mol)**		**ΔH^0(kcal/mol)**		**ΔG^0(kcal/mol)**	
	Gas	solvent	Gas	solvent	Gas	solvent	Gas	solvent
B2PLYP	-5.8	-3.4	-6.2	-4.1	-6.2	-4.1	-4.0	-1.9
B3LYP	-3.5	-0.8	-3.8	-1.5	-3.8	-1.5	-1.6	0.7
BLYP	-2.8	-0.2	-3.3	-1.0	-3.3	-1.0	-1.3	1.1
M05	-1.1	0.6	-1.3	0.4	-1.3	0.4	0.8	2.7
M06	-3.2	-0.7	-3.2	-0.9	-3.3	-0.9	-1.3	1.1
SVWN	-9.7	-6.8	-10.4	-7.8	-10.4	-7.8	-8.0	-5.1
TPSS	-3.2	-0.6	-3.8	-1.4	-3.8	-1.4	-2.0	0.8
ωB97	-2.4	-0.2	-2.7	-0.7	-2.7	-0.7	-0.3	1.6
ωB97X	-3	-0.7	-3.2	-1.2	-3.2	-1.2	-0.9	0.8
ωB97X-D	-4.3	-1.9	-4.5	-2.3	-4.5	-2.3	-2.1	0.1

Table. **VI.7**. Thermodynamic values (kcal/mol) of the condensation reactions to form the enol tautomer **7** in gas phase and in CH_2Cl_2 (IEF-PCM) as calculated at the DFT level with different XC and the cc-pVTZ basis set.

Functional	**ΔE^0(kcal/mol)**		**ΔU^0(kcal/mol)**		**ΔH^0(kcal/mol)**		**ΔG^0(kcal/mol)**	
	Gas	solvent	Gas	solvent	Gas	solvent	Gas	solvent
B2PLYP	-1.4	-0.4	-2.0	-1.1	-2.0	-1.1	0.2	1.1
B3LYP	1.0	2.2	0.5	1.5	0.4	1.5	2.6	3.8
BLYP	1.3	2.6	0.6	1.8	0.6	1.7	2.6	3.9
M05	3.4	3.8	3.0	3.5	3.0	3.5	5.1	5.8
M06	1.3	2.4	1.1	2.1	1.1	2.1	3.3	4.6
SVWN	-5.5	-4.2	-6.5	-5.5	-6.5	-5.5	-5.1	-3.1
TPSS	1	2.2	0.2	1.3	0.2	1.3	2.1	3.6
ωB97	2.2	3.1	1.8	2.7	1.8	2.7	4.1	5.2
ωB97X	1.6	2.6	1.2	2.1	1.2	2.1	3.6	4.5
ωB97X-D	0.1	1.2	-0.2	0.8	-0.2	0.7	2.2	3.2

Table. **VI.8**. Thermodynamic values (kcal/mol) of the condensation reactions to form the enol tautomer **8** in gas phase and in CH_2Cl_2 (IEF-PCM) as calculated at the DFT level with different XC and the cc-pVTZ basis set.

Functional	**ΔE^0(kcal/mol)**		**ΔU^0(kcal/mol)**		**ΔH^0(kcal/mol)**		**ΔG^0(kcal/mol)**	
	Gas	solvent	Gas	solvent	Gas	solvent	Gas	solvent
B2PLYP	-8.1	-6.2	-8.5	-6.8	-8.5	-6.8	-6.1	-4.6
B3LYP	-5.8	-3.7	-6.1	-4.3	-6.1	-4.3	-3.8	-2.1
BLYP	-5.0	-2.8	-5.4	-3.5	-5.4	-3.5	-3.3	-1.4
M05	-3.7	-2.8	-3.9	-2.7	-3.9	-2.7	-1.7	-0.4
M06	-5.7	-3.7	-5.7	-3.9	-5.7	-3.9	-3.7	-2.0
SVWN	-12.1	-9.8	-12.8	-10.8	-12.8	-10.7	-10.6	-8.3
TPSS	-5.5	-3.5	-6.0	-4.1	-6.0	-4.1	-4.0	-1.9
ωB97	-5.2	-3.4	-5.5	-3.9	-5.5	-3.9	-2.9	-1.5
ωB97X	-5.7	-3.8	-5.9	-4.3	-5.9	-4.3	-3.4	-2.2
ωB97X-D	-6.9	-4.9	-7.0	-5.3	-7.0	-5.3	-4.5	-2.9

Table. **VI.9**. Thermodynamic values (kcal/mol) of the condensation reactions to form the enol tautomer **9** in gas phase and in CH_2Cl_2 (IEF-PCM) as calculated at the DFT level with different XC and the cc-pVTZ basis set.

Functional	**ΔE^0(kcal/mol)**		**ΔU^0(kcal/mol)**		**ΔH^0(kcal/mol)**		**ΔG^0(kcal/mol)**	
	Gas	solvent	Gas	solvent	Gas	solvent	Gas	solvent
B2PLYP	-2.2	-1.8	-2.8	-2.6	-2.8	-2.6	-1.1	-1.0
B3LYP	0.0	0.7	-0.6	-0.1	-0.6	-0.1	1.4	1.5
BLYP	0.4	1.1	-0.3	0.2	-0.3	0.2	1.5	1.9
M05	2.9	2.8	2.5	2.4	2.5	2.4	4.4	4.6
M06	0.5	1.0	0.3	0.7	0.3	0.7	2.0	2.5
SVWN	-7.0	-6.5	-8.3	-8.0	-8.0	-8.0	-6.0	-5.3
TPSS	-0.2	0.5	-1.0	-0.5	-1.0	-0.5	0.8	1.5
ωB97	1.7	2.0	1.2	1.5	1.2	1.5	3.3	3.7
ωB97X	1.0	1.4	0.6	0.9	0.6	0.9	2.6	2.5
ωB97X-D	-0.4	0.1	-0.7	-1.1	-0.7	-1.1	1.1	2.1

Table. **VI.10**: Linear regressions related to Fig. **IV.5**

Functionals	Equation	R^2
	Isolated molecules	
MP2	$\Delta E^0_{MP2} = 0.9477\Delta E^0_{CCSD}+4.6272$	0.9919
B2PLYP	$\Delta E^0_{B2PLYP} = 0.9772\ \Delta E^0_{CCSD}+0.7148$	0.9956
B3LYP	$\Delta E^0_{B3LYP} = 0.9718\Delta E^0_{CCSD} +3.0299$	0.9931
BLYP	$\Delta E^0_{BLYP} = 0.9162\ \Delta E^0_{CCSD} +3.2587$	0.9906
M05	$\Delta E^0_{M05} = 0.9893\ \Delta E^0_{CCSD} +5.6283$	0.9875
M06	$\Delta E^0_{M06} = 0.9941\Delta E^0_{CCSD} +3.4499$	0.9926
SVWN	$\Delta E^0_{SVWN} = 0.9607\Delta E^0_{CCSD} - 3.6303s$	0.9661
TPSS	$\Delta E^0_{TPSS} = 0.9306\Delta E^0_{CCSD} +2.8577$	0.9886
ωB97	$\Delta E^0_{\omega B97} = 1.0303\ \Delta E^0_{CCSD} +4.4963$	0.9916
ωB97X	$\Delta E^0_{\omega B97X} = 1.0161\Delta E^0_{CCSD} +3.8304$	0.9928
ωB97X-D	$\Delta E^0_{\omega B97X-D} = 0.9606\Delta E^0_{CCSD}+2.1839$	0.9908
	CH_2Cl_2	
MP2	$\Delta E^0_{MP2} = 0.9401\ \Delta E^0_{CCSD} -4.4387$	0.9974
B2PLYP	$\Delta E^0_{B2PLYP} =0.9854\ \Delta E^0_{CCSD} + 1.4198$	0.9911
B3LYP	$\Delta E^0_{BLYP} =0.9853\Delta E^0_{CCSD} +3.9904$	0.9876
BLYP	$\Delta E^0_{LYP}= 0.9228\Delta E^0_{CCSD} +4.2636$	0.9773
M05	$\Delta E^0_{M05} = 1.026\Delta E^0_{CCSD} + 5.3205$	0.9764
M06	$\Delta E^0_{M06}= 1.0156\ \Delta E^0_{CCSD} + 4.3428$	0.9889
SVWN	$\Delta E^0_{SVWN}= 1.0019\Delta E^0_{CCSD} -2.5624$	0.9119
TPSS	$\Delta E^0_{TPSS} = 0.9629\ \Delta E^0_{CCSD} +3.8959$	0.9632
ωB97	$\Delta E^0_{\omega B97} = 1.0494\Delta E^0_{CCSD} +5.1806$	0.9900
ωB97X	$\Delta E^0_{\omega B97X} = 1.0337\Delta E^0_{CCSD} + 4.5634$	0.9917
ωB97X-D	$\Delta E^0_{\omega B97X-D} = 1.0363\Delta E^0_{CCSD} +3.2669$	0.9845

Table. **VI.11**: Linear regressions related to Fig. **IV.6**

Functionals	Equation	R^2
	Isolated molecules	
B2PLYP	$\Delta H^0_{B2PLYP} = 1.018\ \Delta H^0_{MP2}+5.3753$	0.9910
B3LYP	$\Delta H^0_{B3LYP} = 1.0133\Delta H^0_{MP2} +7.706$	0.9870
BLYP	$\Delta H^0_{BLYP} = 0.9512\ \Delta H^0_{MP2} +7.4804$	0.9878
M05	$\Delta H^0_{M05} = 1.038\Delta H^0_{MP2} +10.581$	0.9752
M06	$\Delta H^0_{M06} = 1.0449\Delta H^0_{MP2} +8.6366$	0.9854
SVWN	$\Delta H^0_{SVWN} = 1.0041\Delta H^0_{MP2} +0.4977$	0.9592
TPSS	$\Delta H^0_{TPSS} = 0.9642\Delta H^0_{MP2}+7.025$	0.9840
ωB97	$\Delta H^0_{\omega B97} = 1.0761\Delta H^0_{MP2}+9.6188$	0.9744
ωB97X	$\Delta H^0_{\omega B97X} = 1.0644\Delta H^0_{MP2} +8.962$	0.9794
ωB97X-D	$\Delta H^0_{\omega B97X-D} = 1.043\Delta H^0_{MP2}+7.4226$	0.9847
	CH_2Cl_2	
B2PLYP	$\Delta H^0_{B2PLYP} = 1.0297\ \Delta H^0_{MP2}+5.9066$	0.9869
B3LYP	$\Delta H^0_{B3LYP} = 1.0275\Delta H^0_{MP2} +8.4378$	0.9817
BLYP	$\Delta H^0_{BLYP} = 0.9679\ \Delta H^0_{MP2} +8.3475$	0.9846
M05	$\Delta H^0_{M05} = 1.0635\Delta H^0_{MP2} +10.869$	0.9623
M06	$\Delta H^0_{M06} = 1.0656\Delta H^0_{MP2} +9.3962$	0.9781
SVWN	$\Delta H^0_{SVWN} = 1.0517\Delta H^0_{MP2} +1.5747$	0.9229
TPSS	$\Delta H^0_{TPSS} = 0.9932\Delta H^0_{MP2}+8.005$	0.9795
ωB97	$\Delta H^0_{\omega B97} = 1.0933\Delta H^0_{MP2}+10.156$	0.9505
ωB97X	$\Delta H^0_{\omega B97X} = 1.0831\Delta H^0_{MP2} +9.5199$	0.9625
ωB97X-D	$\Delta H^0_{\omega B97X-D} = 1.1068\Delta H^0_{MP2} +8.3321$	0.9375

Table. **VI.12**: Linear regressions related to Fig. **IV.7**

Functionals	Equation	R^2
	Isolated molecules	
B2PLYP	$\Delta G^0_{B2PLYP} = 1.0212\Delta G^0_{MP2}+5.1327$	0.9886
B3LYP	$\Delta G^0_{B3LYP} =1.0253\ \Delta G^0_{MP2} +7.5813$	0.9855
BLYP	$\Delta G^0_{BLYP} = 0.9634\Delta G^0_{MP2} +7.318$	0.9892
M05	$\Delta G^0_{M05} = 1.049\Delta G^0_{MP2} +10.319$	0.9720
M06	$\Delta G^0_{M06} = 1.0659\Delta G^0_{MP2} +8.3464$	0.9796
SVWN	$\Delta G^0_{SVWN} = 1.0142\Delta G^0_{MP2} +0.2906$	0.9722
TPSS	$\Delta G^0_{TPSS} = 0.9734\Delta G^0_{MP2}+6.7496$	0.9876
ωB97	$\Delta G^0_{\omega B97} = 1.072\Delta G^0_{MP2}+9.3542$	0.9716
ωB97X	$\Delta G^0_{\omega B97X} = 1.0673\Delta G^0_{MP2} +8.7514$	0.97.55
ωB97X-D	$\Delta G^0_{\omega B97X-D} = 1.0723\Delta G^0_{MP2}+7.4351$	0.9876
	CH_2Cl_2	
B2PLYP	$\Delta G^0_{B2PLYP} = 1.0284\Delta G^0_{MP2}+5.4273$	0.9783
B3LYP	$\Delta G^0_{B3LYP} = 1.035\Delta G^0_{MP2} +8.0479$	0.9703
BLYP	$\Delta G^0_{BLYP} = 0.9668\Delta G^0_{MP2} +7.9636$	0.9806
M05	$\Delta G^0_{M05} = 1.0772\ \Delta G^0_{MP2} +10.586$	0.9620
M06	$\Delta G^0_{M06} = 1.1349\Delta G^0_{MP2} +9.3381$	0.9731
SVWN	$\Delta G^0_{SVWN} = 1.1028\Delta G^0_{MP2} +1.8721$	0.9414
TPSS	$\Delta G^0_{TPSS} = 1.0225\Delta G^0_{MP2}+7.9141$	0.9762
ωB97	$\Delta G^0_{\omega B97} = 1.0906\Delta G^0_{MP2}+9.7206$	0.9494
ωB97X	$\Delta G^0_{\omega B97X} = 1.1023\Delta G^0_{MP2} +9.0203$	0.9606
ωB97X-D	$\Delta G^0_{\omega B97X-D} = 1.192\Delta G^0_{MP2}+8.6719$	0.9619

Table. **VI.13**: Linear regressions related to Fig. **IV.8**

Functionals	Equation	R^2
	Isolated molecules	
B2PLYP	$\Delta S^0_{B2PLYP} = 1.1718\ \Delta S^0_{MP2} +2.0832$	0.9832
B3LYP	$\Delta S^0_{B3LYP} = 0.878\ \Delta S^0_{MP2} - 0.2573$	0.9639
BLYP	$\Delta S^0_{BLYP} = 0.9048\ \Delta S^0_{MP2} +0.5547$	0.9466
M05	$\Delta S^0_{M05} = 0.8905\ \Delta S^0_{MP2} +0.084$	0.9105
M06	$\Delta S^0_{M06} = 0.7865\Delta S^0_{MP2} - 0.3729$	0.8860
SVWN	$\Delta S^0_{SVWN} = 0.8735\Delta S^0_{MP2} - 0.3344$	0.7192
TPSS	$\Delta S^0_{TPSS} = 0.6827\Delta S^0_{MP2} - 0.9495$	0.8720
ωB97	$\Delta S^0_{\omega B97} = 0.9715\ \Delta S^0_{MP2} - 0.0321$	0.9651
ωB97X	$\Delta S^0_{\omega B97X} = 0.9248\Delta S^0_{MP2} – 0.2714$	0.9567
ωB97X-D	$\Delta S^0_{\omega B97X-D} = 1.259\Delta S^0_{MP2} +2.4448$	0.9314
	CH_2Cl_2	
B2PLYP	$\Delta S^0_{B2PLYP} = 1.6705\ \Delta S^0_{MP2} + 6.6724$	0.8771
B3LYP	$\Delta S^0_{B3LYP} = 1.7723\Delta S^0_{MP2} +7.4388$	0.8892
BLYP	$\Delta S^0_{BLYP}= 1.1766\ \Delta S^0_{MP2} +2.9185$	0.9246
M05	$\Delta S^0_{M05} = 1.1319\ \Delta S^0_{MP2} + 1.7258$	0.6271
M06	$\Delta S^0_{M06}= 1.3071\ \Delta S^0_{MP2} + 3.9716$	0.6756
SVWN	$\Delta S^0_{SVWN}= 1.0798\ \Delta S^0_{MP2} + 0.5980$	0.4012
TPSS	$\Delta S^0_{TPSS} = 0.8542\ \Delta S^0_{MP2} - 0.1738$	0.7698
ωB97	$\Delta S^0_{\omega B97} = 1.125\ \Delta S^0_{MP2} + 1.5153$	0.7764
ωB97X	$\Delta S^0_{\omega B97X} = 1.3532\ \Delta S^0_{MP2} + 4.3167$	0.7784
ωB97X-D	$\Delta S^0_{\omega B97X-D} = 1.4814\ \Delta S^0_{MP2} + 4.4632$	0.8675

VII. References

1. Sauer, M., Yeung, C., Chong, J. H., Patrick, B. O. & Maclachlan, M. J. N -Salicylideneanilines : Tautomers for Formation of Hydrogen-Bonded Capsules , Clefts , and Chains. 775–788 (2006).

2. Charette, J. J. & De Hoffmann, E. Physicochemical Properties of Schiff Bases. 4. Tautomeric Equilibrium and Kinetics of Hydrolysis of N-Benzylideneaniline Derivatives. *J. Org. Chem.* **44**, 2256–2262 (1979).

3. Ogawa, K., Harada, J., Tamura, I. & Noda, Y. X-ray crystallographic analysis of the NH form of a salicylideneaniline at 15 K. *Chem. Lett.* 528–529 (2000). doi:10.1246/cl.2000.528

4. Sauer, M., Yeung, C., Chong, J. H., Patrick, B. O. & MacLachlan, M. J. N-salicylideneanilines: Tautomers for formation of hydrogen-bonded capsules, clefts, and chains. *J. Org. Chem.* **71**, 775–788 (2006).

5. Johmoto, K., Sekine, A. & Uekusa, H. Photochromism Control of Salicylideneaniline Derivatives by Acid− Base Co-Crystallization. (2012). doi:10.1021/cg300454q

6. Carletta, A., Buol, X., Leyssens, T., Champagne, B. & Wouters, J. Polymorphic and Isomorphic Cocrystals of a N-Salicylidene-3-aminopyridine with Dicarboxylic Acids: Tuning of Solid-State Photo- and Thermochromism. *J. Phys. Chem. C* **120**, 10001–10008 (2016).

7. Universit, R. Engineering N -salicylidene aniline derivatives : from solid-state molecular switches to multifunctional organic-inorganic architectures.

8. Miura, M., Harada, J. & Ogawa, K. Temperature-Induced Reversal of Proton Tautomerism : Role of Hydrogen Bonding and Aggregation in 7-Hydroxyquinolines. 9854–9858 (2007). doi:10.1021/jp073909d

9. Mahmoodi, N. O., Aghajani, N. & Ghavidast, A. Synthesis and photochromic properties of thiolated N-salicylidene-anilines on silver nanoparticles. *J. Mol. Struct.* **1128**, 21–29 (2017).

10. Enol, K. *et al.* Investigation on the Second-Order Nonlinear Optical Responses in the. 5638–5645 (2008). doi:10.1021/jp711511t

11. Baleiza, C. Chiral Salen Complexes : An Overview to Recoverable and Reusable Homogeneous and Heterogeneous Catalysts. (2006). doi:10.1021/cr050973n

12. Bosnerb, B. The Schiff bases of salicylaldehyde and aminopyridines as highly sensitive analytical reagents. **343**, 145–153 (1997).

13. Jochum, F. D. & Theato, P. Temperature- and Light-Responsive Polyacrylamides Prepared by a Double Polymer Analogous Reaction of Activated Ester Polymers. 5941–5945 (2009). doi:10.1021/ma900945s

14. Feringa, B. E. N. L. In Control of Motion : From Molecular Switches to Molecular Motors †. **34**, 504–513 (2001).

15. Hadjoudis, E. R1. 301–337 (1995).

16. Amimoto, K. & Kawato, T. Photochromism of organic compounds in the crystal state. **6**, 207–226 (2006).

17. Sherrill, C. D. An Introduction to Hartree-Fock Molecular Orbital Theory What Problem Are We Solving ? Motivation and the Hartree Product. *Sch. Chem. Biochem. Georg. Inst. Technol.* 1–8 (2000).

18. Charlotte Froese Fischer - The Hartree-Fock Method for Atoms_ A Numerical Approach (1977,

John Wiley & Sons Inc) - libgen.

19. Method, T. H. E. H. & Determinant, T. H. E. S. Lecture IV : The Hartree-Fock method. **1**, 1–9

20. Weeks, D. P. C. C. L. E. Y. N. to K. in 20. *CHALLENGES AND ADVANCES IN COMPUTATIONAL CHEMISTRY AND PHYSICS*. *Dk* **53**, (2015).

21. Kaufman, G. B. Inorganic chemistry: principles of structure and reactivity, 4th ed. (Huheey, James E.; Keiter, Ellen A.; Keiter, Richard L.). *J. Chem. Educ.* **70**, A279 (1993).

22. Zerner, M. C. Perspective on "New developments in molecular orbital theory". in *Theoretical Chemistry Accounts* 217–218 (Springer Berlin Heidelberg, 2000). doi:10.1007/978-3-662-10421-7_15

23. Schuchardt, K. L. *et al.* Basis set exchange: A community database for computational sciences. *J. Chem. Inf. Model.* **47**, 1045–1052 (2007).

24. Koch, W. & Holthausen, M. C. *A Chemist's Guide to Density Functional Theory*. *A Chemist's Guide to Density Functional Theory* (Wiley, 2001). doi:10.1002/3527600043

25. Dunning, T. H. Gaussian basis sets for use in correlated molecular calculations. I. The atoms boron through neon and hydrogen. *J. Chem. Phys.* **90**, 1007–1023 (1989).

26. Cremer, D. From configuration interaction to coupled cluster theory: The quadratic configuration interaction approach. *Wiley Interdiscip. Rev. Comput. Mol. Sci.* **3**, 482–503 (2013).

27. Shavitt, I. The Method 01 Configuration Interaction.

28. Cremer, D. Møller-Plesset perturbation theory: From small molecule methods to methods for thousands of atoms. *Wiley Interdiscip. Rev. Comput. Mol. Sci.* **1**, 509–530 (2011).

29. Mller, C. & PLEsSET, M. S. *Note on an Approximation Treatment for Many-Electron Systems*. (1934).

30. Møller - Plesset many body perturbation theory. (2015).

31. Krishnan, R. & Pople, J. A. Approximate fourth-order perturbation theory of the electron correlation energy. *Int. J. Quantum Chem.* **14**, 91–100 (1978).

32. Pople, J. A., Binkley, J. S. & Seeger, R. Theoretical models incorporating electron correlation. *Int. J. Quantum Chem.* **10**, 1–19 (1976).

33. Pople, J. A., Seeger, R. & Krishnan, R. Variational configuration interaction methods and comparison with perturbation theory. *Int. J. Quantum Chem.* **12**, 149–163 (1977).

34. Head-Gordon, M., Pople, J. A. & Frisch, M. J. MP2 energy evaluation by direct methods. *Chem. Phys. Lett.* **153**, 503–506 (1988).

35. Leininger, M. L., Allen, W. D., Schaefer, H. F. & Sherrill, C. D. Is Moller - Plesset perturbation theory a convergent ab initio method? *J. Chem. Phys.* **112**, 9213–9222 (2000).

36. Handy, N. C. & Schaefer, H. F. On the evaluation of analytic energy derivatives for correlated wave functions. *J. Chem. Phys.* **81**, 5031–5033 (1984).

37. Zhang, I. Y. & Grüneis, A. Coupled cluster theory in materials science. *Front. Mater.* **6**, (2019).

38. Čížek, J. On the Correlation Problem in Atomic and Molecular Systems. Calculation of Wavefunction Components in Ursell-Type Expansion Using Quantum-Field Theoretical Methods. *J. Chem. Phys.* **45**, 4256–4266 (1966).

39. Tsuneda, T. *Density Functional Theory in Quantum Chemistry*. *Density Functional Theory in*

Quantum Chemistry (2014). doi:10.1007/978-4-431-54825-6

40. Hasnip, P. J. *et al.* Density functional theory in the solid state. *Philos. Trans. R. Soc. A Math. Phys. Eng. Sci.* **372**, (2014).

41. Kohn, W. Fundamentals of density functional theory. in *Density Functionals: Theory and Applications* 1–7 (Springer Berlin Heidelberg, 2008). doi:10.1007/bfb0106731

42. [International series of monographs on chemistry 16] Robert G.

43. Kohn, W. & Sham, L. J. Self-Consistent Equations Including Exchange and Correlation Effects. *Phys. Rev.* **140**, A1133–A1138 (1965).

44. Bistafa Da Silva, C. E. *Efeito de Solvente no Espectro de Absorção da 5-Fluorouracil. Análise de Diferentes Procedimentos Teóricos*.

45. Kirkwood, J. G. Theory of solutions of molecules containing widely separated charges with special application to zwitterions. *J. Chem. Phys.* **2**, 351–361 (1934).

46. Onsagbr, L. & 58, V. *Electric Moments of*.

47. Tapia, O. & Goscinski, O. Self-consistent reaction field theory of solvent effects. *Mol. Phys.* **29**, 1653–1661 (1975).

48. Rivail, J. L. & Rinaldi, D. A quantum chemical approach to dielectric solvent effects in molecular liquids. *Chem. Phys.* **18**, 233–242 (1976).

49. Silva, C. E. B. da. Efeito de solvente no espectro de absorção da 5-fluorouracil. Análise de diferentes procedimentos teóricos. (Biblioteca Digital de Teses e Dissertações da Universidade de São Paulo, 2011). doi:10.11606/D.43.2011.tde-31032011-134135

50. Böttcher, C. J. F., van Belle, O. C., Bordewijk, P., Rip, A. & Yue, D. D. Theory of Electric Polarization. *J. Electrochem. Soc.* **121**, 211C (1974).

51. Cheung, D. L. G. Structures and properties of liquid crystals and related molecules from computer simulation. (2002).

52. Gaussian 16, Revision C.01, M. J. Frisch, G. W. Trucks, H. B. Schlegel, ... J. B. Foresman, and D. J. Fox, Gaussian, Inc., Wallingford CT, 2016.

53. Inc, J. O.-G. & 2000, undefined. Thermochemistry in gaussian. *courses.chem.psu.edu*

54. Carletta, A., Buol, X., Leyssens, T., Champagne, B. & Wouters, J. Polymorphic and Isomorphic Cocrystals of a N-Salicylidene-3-aminopyridine with Dicarboxylic Acids: Tuning of Solid-State Photo-and Thermochromism. *J. Pjhys. Chem. C.* **120**, 10001–10008 (2016).

UNIVERSITÉ CATHOLIQUE DE LOUVAIN
École polytechnique de Louvain
Rue Archimède, 1 bte L6.11.01, 1348 Louvain-la-Neuve, Belgique | **www.uclouvain.be/epl**